In vitro and *in silico* investigation of water-soluble fullerenol $C_{60}(OH)_{24}$: bioactivity and biocompatibility

Vladimir V. Sharoyko[a,b,c*], Nailia R. Iamalova[a,d], Sergei V. Ageev[a,b], Anatolii A. Meshcheriakov[a,b], Gleb O. Iurev[a,e], Andrey V. Petrov[b], Dmitry A. Nerukh[f], Vladimir S. Farafonov[g], Lubov V. Vasina[a], Anastasia V. Penkova[b], Konstantin N. Semenov[a,b,c*]

[a]Pavlov First Saint Petersburg State Medical University, 6–8 L'va Tolstogo ulitsa, Saint Petersburg, 197022, Russia

[b]Institute of Chemistry, Saint Petersburg State University, 26 Universitetskii prospekt, Saint Petersburg, 198504, Russia

[c]A. M. Granov Russian Research Centre for Radiology and Surgical Technologies, 70 Leningradskaya Ulitsa, Saint Petersburg, 197758, Russia

[d]Agrophysical Research Institute, 14 Grazhdanskii prospect, Saint Petersburg 195220, Russia

[e]Almazov National Medical Research Centre, 2 Akkuratova ulitsa, Saint Petersburg, 197341, Russia

[f]Department of Mathematics, Aston University, Birmingham, B4 7ET, UK

[g]V. N. Karazin Kharkiv National University, 4 Svobody ploshchad', Kharkiv, 61022, Ukraine

[*]Corresponding authors at: 6–8 L'va Tolstogo ulitsa, Saint Petersburg, 197022, Russia (K. N. Semenov) and 26 Universitetskii prospekt, Saint Petersburg, 198504, Russia (V. V. Sharoyko)

E-mail addresses: knsemenov@gmail.com (K. N. Semenov), sharoyko@gmail.com (V. V. Sharoyko).

Abstract

Light fullerenes, C_{60} and C_{70}, have significant potential in biomedical applications due to their ability to absorb reactive oxygen species, inhibit the development of tumours, inactivate viruses and bacteria, and as the basis for developing systems for targeted drug delivery. However, the hydrophobicity of individual fullerenes complicates their practical use, therefore, creating water-soluble derivatives of fullerenes is increasingly important. Currently, the most studied soluble adducts of fullerenes are polyhydroxyfullerenes or fullerenols. Unfortunately, investigations of fullerenol biocompatibility are fragmental. They often lack reproducibility both in the synthesis of the compounds and their biological action. We here investigate the biocompatibility of a well-defined fullerenol $C_{60}(OH)_{24}$ obtained using methods that minimise the content of impurities and quantitatively characterise the product's composition. We carry out comprehensive biochemical and biophysical investigations of $C_{60}(OH)_{24}$ that include photodynamic properties, cyto- and genotoxicity, haemocompatibility (spontaneous and photoinduced haemolysis, platelet aggregation), the thermodynamic characteristics of $C_{60}(OH)_{24}$ binding to human serum albumin and DNA. The performed studies show good biocompatibility of fullerenol $C_{60}(OH)_{24}$, which makes it a promising object for potential use in biomedicine.

Keywords: Fullerenol; HSA; Cytotoxicity; Genotoxicity; Haemolysis; Molecular Dynamics.

1. Introduction

Polyhydroxylated fullerenes (fullerenols) are currently the most studied class of water-soluble derivatives of fullerenes [1–6]. Fullerenols exhibit high antioxidant activity, radioprotective, antimutagenic, antitumour, and antimetastatic properties [7–16]. Due to their low toxicity [1,17–21] and chemical structure convenient for immobilisation of various biologically active molecules, fullerenols are promising drug carriers [17,22–25].

Saitoh *et al.* [10] studied the possibility of using the fullerenol $C_{60}(OH)_{24}$ as a radioprotector and found that it prevents the radiation-induced decrease in leukocyte level, and that it exhibits radioprotective properties most effectively in the spleen, small intestine, and lungs of rats.

The antioxidant properties of fullerenols were first described under the conditions of inducing reactive oxygen species (ROS) production caused by the reversible damage to hippocampus for *in vitro* [26], as well as *in vivo* models of dogs with intestinal ischemia-reperfusion and small bowel transplantation [27]. It was later shown that $C_{60}(OH)_{24}$ can trap the radicals of nitrogen monoxide when sodium nitroprusside (NO radicals donor) is added to the solution [9]. In recent studies, a correlation was found between the antioxidant properties of $C_{60}(OH)_{24}$ and the activity of nuclear factor erythroid 2-related factor 2 (NRF2), which regulates the expression of antioxidant enzymes [28].

Fullerenes can be used as photosensitisers. The ability of fullerene C_{60} and its water-soluble derivative $C_{60}(OH)_{18}$ to damage cell membranes after photoactivation was studied with rat liver microsomes. It was shown that fullerene and fullerenol can generate ROS as a result of photoexcitation and cause lipid peroxidation and oxidation of cell membrane proteins [29].

Another application of fullerenols, associated with the delivery of anticancer drugs, was proposed in ref. [24]. The fullerenol-doxorubicin conjugate ($C_{60}(OH)_{18–24}$–Dox) inhibited *in vitro* proliferation of tumour cell lines (mouse melanoma B16–F10, mouse lung carcinoma LLC1,

and metastatic human breast carcinoma MDA-MB231) by blocking the G2-M cell cycle phase leading to apoptosis. *In vivo* experiments in mice showed high antitumour efficacy of the fullerenol-Dox conjugate without the systemic toxicity of free Dox.

The protective function of $C_{60}(OH)_{24}$ against Dox-induced hepatotoxicity in experiments was studied *in vivo* (using Sprague Dawley rats) and *in vitro* (using human HepG2 hepatocellular carcinoma and Caco-2 colorectal adenocarcinoma) [30]. The authors found that it can serve as a potential hepatoprotector under the conditions of Dox-induced hepatotoxicity.

Xu *et al.* [31] found that the fullerenols $C_{60}(OH)_x$ (x = 22, 24) can reduce the toxic effects of some dangerous toxicants. For example, a model based on hepato- and nephrotoxicity, caused by the action of carbon tetrachloride (CCl_4), was used to study the protective mechanisms of fullerenol in Sprague Dawley rats. It was found that liver and kidney were protected against CCl_4-induced oxidative stress by activating the antioxidant defence systems.

Fullerenols have a positive effect on the development, yield, and quality of various crops. Panova *et al.* [32] and Bityutskii *et al.* [33] developed nanocompositions containing fullerenols $C_{60}(OH)_{n1}O_{n2}$ and various trace elements that led to increased crop yields, improved crop quality, reduced ripening period of fruits and vegetables, reduced degree of diseases damage to plants, increased plant resistance to adverse environmental conditions (winter hardness, drought tolerance), increased seed germination, and reduced level of nitrates in plants.

Summarising, fullerenols are the most studied class of water-soluble fullerene derivatives. The study of this class of compounds began more than 20 years ago and to date a fairly large array of information has been accumulated on the production, the physicochemical and biological properties, as well as on the use of fullerenols. However, literature on the biological properties and biocompatibility of water-soluble fullerene derivatives shows systematic limitations in their studies. They include the following:

1. Most studies lack comprehensive data on the quantitative identification of fullerenols.

2. The proposed synthesis methods often do not provide compounds with a reproducible composition of the final product.

3. It is known that in addition to hydroxyl groups, fullerenols may contain other functional groups (oxo, epoxy, carboxy, etc.); it should also be noted that most of the methods for the synthesis of fullerenols are carried out in alkaline medium [3,34–36], thus, fullerenols can exist in the form of salts.

4. The studies of the biological properties and biocompatibility of fullerenols are fragmentary. The reason is low reproducibility of the composition of the studied adducts (see the points above).

All this makes it very difficult to investigate the biomolecular mechanisms of fullerenols' action.

We address the above deficiencies in the present work and report on the studies of the biocompatibility of the well-defined fullerenol $C_{60}(OH)_{24}$. This adduct was obtained under mild conditions by alkaline hydrolysis of a bromo derivative $C_{60}Br_{24}$. The use of this technique made it possible to obtain a reproducible composition of the final product with a minimum content of impurity groups [9,37–39]. Thus, in this work, for the first time, a comprehensive study of the biocompatibility of $C_{60}(OH)_{24}$ aqueous solutions was carried out.

The study of biocompatibility is a key point for preclinical studies and a starting point for further applications of this adduct in nanobiomedicine. No doubt, the uniqueness of the electronic structure of fullerenols, its compatibility with water and aqueous solutions, the presence of an internal volume, and the possibility of immobilisation of biologically active molecules make this class of compounds extremely promising for biology and medicine. Here we investigate the thermodynamic characteristics of the binding of fullerenol to human serum albumin (HSA) and DNA, genotoxicity, platelet aggregation, erythrocyte haemolysis

(spontaneous and photo-induced), and photodynamic properties. As the first step in the investigation of biomolecular mechanisms behind the fullerenols' activity, the molecular dynamics (MD) simulations were carried out to study the process of $C_{60}(OH)_{24}$ self-association in water, as well as the interaction of $C_{60}(OH)_{24}$ with HSA.

2. Experimental part

2.1 Materials

The manufacturers and the purity of the reagents that were used are presented in Table 1. The identification of obtained $C_{60}(OH)_{24}$ using various physicochemical methods (NMR, IR, UV/Vis spectroscopy, mass spectrometry, elemental analysis) was previously described in [40,41].

2.2 Particle size distribution in aqueous solutions and ζ-potentials of $C_{60}(OH)_{24}$

The size distribution of $C_{60}(OH)_{24}$ particles in aqueous solutions in the concentration range C = 10–100 μM was measured using the Malvern Zetasizer 3000 instrument at 293.15 K temperature; the values of polydispersity indices were 0.24–0.47.

Table 2 shows the results for the particle distribution by size and ζ-potentials. The data shows that in the concentration range C = 10–100 μM, the hydrodynamic diameter of the particles in solution increases from 10 to 40 nm. This is most probably due to the self-association of $C_{60}(OH)_{24}$ molecules *via* hydrogen bonds and hydrophobic interactions. The concentration dependence of ζ-potentials shows that in this concentration range the solutions of $C_{60}(OH)_{24}$ are electrokinetically stable.

2.3. Biocompatibility of fullerenol $C_{60}(OH)_{24}$

2.3.1. Erythrocytes haemolysis

Erythrocyte haemolysis was studied by measuring the optical density of supernatants at the wavelength of λ = 540 nm using the SF-2000 spectrophotometer (OKB SPECTR, Russia), as previously described in [42].

1.5 ml of the test mixture was prepared from 750 μl of the $C_{60}(OH)_{24}$ solution with C = 20–200 μM and 750 μl of the suspension of erythrocytes in physiological saline. After the mixture was prepared, the ~~tubes~~ samples were incubated at 37.0 ± 0.2 C for 1 and 3 h and centrifuged for 10 min at 6000 rpm. Erythrocyte suspensions with the addition of equivalent volumes of distilled water and physiological saline, respectively, were used as positive and negative controls. The haematocrit values were in the reference interval of healthy donors (0.40–0.46). The concentration dependence of the relative change in haemolysis was calculated using the following equation:

$$\text{Haemolysis \%} = \frac{A_s - A_0}{A_{100}} \cdot 100\ \% \quad (1),$$

where A_s is the optical density of the sample, A_0 is the optical density of the control, A_{100} is the optical density of water with the suspension of erythrocytes (100 % haemolysis).

2.3.2. Photo-induced haemolysis

Erythrocytes were obtained from citrate blood by centrifugation at 1500 rpm for 10 min, followed by three washing cycles with physiological saline. Then the cells were stabilised for 24 h at 4 °C in Alsever's reagent (2.05 % dextrose, 0.8 % sodium citrate, 0.055 % citric acid, and 0.42 % sodium chloride). Before the experiment, the erythrocytes were washed three times in Alsever's reagent with saline. Washing removed plasma residues, leukocytes, platelets, and electrolytes. Further experiments were carried out with the stabilised suspension of erythrocytes. Then the standard suspension of the erythrocytes with optical density equal to 0.560 ± 0.020 at 800 nm was prepared after eight-fold dilution with phosphate buffer (pH 7.4).

The antioxidant properties of $C_{60}(OH)_{24}$ were evaluated using a device for the study of photoinduced haemolysis by the method published previously [43]. The measurements were performed using the SF 2000 spectrophotometer (Russia) in a cuvette with the optical path length of 5 mm. According to this technique, in a shielded cuvette with the optical path length of 5 mm, the incubation mixture was prepared. The mixture contained 100 μl of the standard

suspension of erythrocytes, 600 μl of the phosphate buffer solution (pH 7.4), 80 μl of the solution with various concentrations of $C_{60}(OH)_{24}$ (C = 10–100 μM), and 20 μl of the photosensitiser Radachlorin (0.35 % solution for intravenous administration, the main substance was (7S, 8S)-13-vinyl-5-(carboxymethyl)-7-(2-carboxyethyl)-2,8,12,17-tetramethyl-18-ethyl-7H,8H-porphyrin-3-carboxylic acid). The final concentration of Radachlorin in the sample was 62.5 $\mu g \cdot ml^{-1}$. As a control, an incubation mixture containing saline instead of fullerenol was used. 800 μl of the resulting incubation mixture was thermostated in the cuvette compartment of the spectrophotometer for 3 min at 37 °C with constant stirring, then it was irradiated with the red Laserland LED-2000 laser (Besram Technology Inc., China; 659 nm, power 55 mW, irradiation dose 3.5 $J \cdot cm^{-2}$). After the completion of irradiation, the decrease in the optical density of the solution at 800 nm was recorded at five-second intervals until complete haemolysis [44].

Using the recorded haemolytic curve, which had a smooth S-shaped character, TC_{50} was determined, the time from the completion of irradiation to lysis of 50 % of erythrocytes in the incubation mixture [43]. By changing the value of TC_{50} the speed of the haemolytic process was estimated.

2.3.3. Effect of $C_{60}(OH)_{24}$ on the haemostasis parameters

Clotting tests include methods for measuring activated partial thromboplastin time (aPTT), prothrombin time (PT), and thrombin time (TT). These methods allow to measure the time interval from the moment of adding a reagent (activator that triggers the clotting process) to the formation of a fibrin clot in the studied plasma.

The effect of $C_{60}(OH)_{24}$ on plasma-coagulation haemostasis was assessed by adding it to plasma in the aPTT, PT, and TT tests. Five donors with normal PT, aPTT, and von Willebrand factor activity were selected.

The principle of the aPTT method is in the study of the plasma recalcification reaction under the conditions of standardisation of the contact and phospholipid activation of blood coagulation. For this purpose, a contact activator (kaolin) and partial thromboplastin, which is functionally similar to platelet phospholipids, are added to plasma. The sensitivity of this test to the deficiency of plasma coagulation factors (excluding factors VII and XIII) is higher than in the test for determining the time of plasma recalcification, but standard phospholipid activation makes it impossible to detect the deficiency of the platelet coagulation activity. The determination of aPTT is a common method of monitoring heparin therapy.

The principle of the PT method consists of determining the clotting time of platelet-poor citrated plasma in the presence of an optimal amount of calcium and excess tissue thromboplastin. This is the variant of determining the time of plasma recalcification with the addition of tissue thromboplastin. In a complex with factor VII and Ca^{2+}, it directly activates factor X, so the test results depend on the activity of factor VII, factor X, and factors involved in the process of blood coagulation at the stages of thrombin and fibrin formation (factors V, II and I).

The TT method is based on the ability of thrombin to induce the conversion of fibrinogen to fibrin without the participation of other blood coagulation factors, i.e. it allows to assess the final stage of blood coagulation (fibrinogen and its derivatives, the activity of factor XIII). Test elongation may indicate the presence of direct anticoagulants in the blood.

To determine aPTT, PT, and TT, we used the APTV-TEST, TEKHPLASTIN-TEST and Trombo-TEST reagent kits from Tekhnologiya-Standart, Russia. The studies were carried out using the APG2-02-P coagulometer (EKMO, Russia). 50 μl of plasma and 50 μl of $C_{60}(OH)_{24}$ solutions (C = 10, 50, 75 and 100 μM) were mixed, incubated at 37 °C for 60 s and, in accordance with the study protocol, the clotting time was determined using the analyser in the aPTT, PT, and TT tests.

2.3.4. Determination of NO-radical uptake

To determine the degree of NO-radicals uptake, the Griess–Ilosvay reaction was used [45]. At physiological pH values, sodium nitroprusside is a donor of NO-radicals, the interaction of which with oxygen leads to the formation of NO_2^-. The nitrite anions formed as a result of the reaction can be detected using the Griess reagent (a pink-violet colour of the solution is observed). For the experiment, the reaction mixture containing 1 ml of sodium nitroprusside (C = 15 μM) and 0.5 ml of the aqueous solution of fullerenol (C = 10–200 μM) was incubated in a shaker thermostat at 100 °C. Then, 0.5 ml of PBS (pH = 7.4) and 0.5 ml of Griess reagent (0.1 % solution in 20 % acetic acid) were added to 0.25 ml of the resulting solution. The obtained mixture was incubated for 30 minutes at room temperature. The formed diazo compound was detected spectrophotometrically at λ = 540 nm. Sodium azide was used as a positive control.

2.3.5. Determination of $C_{60}(OH)_{24}$ reducing capacity

The reducing capacity of $C_{60}(OH)_{24}$ was assessed by the ability of the fullerenol to reduce Fe^{3+} to Fe^{2+} [46]. The reaction mixture containing equal volumes (0.5 ml) of 0.1 % potassium ferricyanide, phosphate buffer (pH = 6.6) and aqueous solutions of the fullerenol with various concentrations (C = 500–1100 μM) was incubated for 20 minutes in a water bath at 50 °C. Then, 0.5 ml of trichloroacetic acid was added to the reaction mixture to terminate the reaction. After that, 1 ml of phosphate buffer (pH = 6.6), and 100 μl of $FeCl_3$ (0.1 %) were added to 1 ml of the resulting solution. The mixture was left at room temperature for 10 minutes. The fullerenol caused the reduction of Fe^{3+} to Fe^{2+} because of its reductive capabilities according to the reaction: $K_3[Fe(CN)_6]$ + Reducing agent ($C_{60}(OH)_{24}$) = $Fe(CN)_6^{4-}$. Prussian blue-coloured complex is formed by adding $FeCl_3$ to Fe^{2+}: $Fe(CN)_6^{4-}$ + $FeCl_3$ → $Fe_4[Fe(CN)_6]_3$. Therefore, the reduction can be determined spectrophotometrically by

measuring the formation of Perl's Prussian blue at 700 nm [47]. In this assay, the yellow colour of the test solution changed to the blue colour. Ascorbic acid was used as a positive control.

2.3.6. Photodynamic properties

To study the photodynamic properties, the absorption spectra of the solutions were obtained: (*i*) Radachlorin; (*ii*) Radachlorin containing $C_{60}(OH)_{24}$ in various concentrations; (*iii*) Radachlorin in the presence of 500 μM sodium azide before and after irradiation with the red Laserland LED-2000 laser. The effect of $C_{60}(OH)_{24}$ on the photobleaching of Radachlorin was evaluated using the photodegradation rate constant k_{deg} [44,48].

2.3.7. Human platelet aggregation

After obtaining informed consent, blood was taken for research from five donors, persons of both sexes aged 20–30, who did not receive drugs affecting platelet function for 7–10 days. To prevent platelet activation, blood was taken in vacuum tubes containing 3.8 % sodium citrate (C = 0.129 M) as a stabiliser in the ratio of sodium citrate to blood equal to 1:9. To obtain platelet rich plasma, the stabilised blood was centrifuged at 1500 rpm for 10 min. Platelet aggregation in platelet-rich plasma was studied using the AP2110 SOLAR aggregometer (Belarus). ADP (final concentration of 10 μM) was used as an aggregation inducer. The plasma samples were incubated at 37 °C before measurements. The aggregation was recorded before the curve reached a plateau.

2.3.8. Identification of the $C_{60}(OH)_{24}$ binding sites at HSA molecule by spectrofluorimetry

The binding of $C_{60}(OH)_{24}$ to HSA was studied using the Tecan Infinite M200 multimode microplate reader spectrofluorometer. The emission spectra were recorded in the wavelength range 310–450 nm at 298.15 K; the excitation wavelength was 290 nm. The HSA concentration was 3 μM, the fullerenol concentration varied in the range C = 0.3–1.5 μM with 0.3 μM step and in the range C = 6.0–24.0 μM with 3.0 μM step. The measurements were

carried out in the absence and in the presence of the following binding site markers: warfarin, ibuprofen, digitonin with the final concentration of C = 3 μM.

2.3.9. Measuring the binding constants of $C_{60}(OH)_{24}$–HSA complex by thermal shift assay (TSA)

Alternatively, the binding of $C_{60}(OH)_{24}$ to HSA was estimated by TSA through measuring the melting point of pure HSA and after the addition of the ligand $C_{60}(OH)_{24}$. 25 μl of a mixture containing HSA (C = 3 μM), 0–100 μM of $C_{60}(OH)_{24}$, and 200x ProteOrange fluorescent dye (Lumiprobe, Russia) was added to PCR tubes in triplicate [49]. The fluorescence data were acquired using the CFX96 Touch Real-Time PCR Instrument (Bio-Rad, USA) with the excitation range of λ = 470–533 nm. The temperature was held for 30 s per degree from 37 °C to 98 °C (~0.5 °C·min^{-1}). The dependencies of the melting points on $C_{60}(OH)_{24}$ concentrations were processed using GraphPad Prism 9.0.0 software, and the dissociation constants for $C_{60}(OH)_{24}$–HSA complex were obtained by approximation [50].

2.3.10. Measurements of esterase activity

To study the effect of $C_{60}(OH)_{24}$ on the esterase activity of HSA, the solutions of 4-nitrophenyl acetate (NPA) in ethanol (1 mg·ml^{-1}), HSA and fullerenol in phosphate buffer (PBS) with pH = 7.02 were prepared. After mixing the solutions, the final concentration of NPA was 100 μM, HSA — 3 μM, the concentration of $C_{60}(OH)_{24}$ varied from 0 to 24 μM. The rate of NPA hydrolysis was recorded by the formation of nitrophenol using the method of initial rates at 405 nm using the Tecan Infinite M200 multimode microplate reader spectrofluorometer.

2.3.11. $C_{60}(OH)_{24}$ binding to DNA

The binding of the $C_{60}(OH)_{24}$ derivative to DNA was studied using the Tecan Infinite M200 multimode microplate reader spectrofluorometer. The DNA concentration was 2.5 μM; the concentration range of $C_{60}(OH)_{24}$ was C = 3–45 μM in 3 μM increments. The solvent used

was phosphate buffered saline (PBS). The emission spectra were recorded in the 360–450 nm wavelength range at the excitation wavelength of 340 nm. The measurements were carried out at 303.15, 308.15, 313.15 and 318.15 K; the thermostat accuracy was ΔT = ±0.01 K. For calculations, the values of the fluorescence intensity at 380 nm were used.

2.3.12. Genotoxicity

The genotoxicity of $C_{60}(OH)_{24}$ was evaluated using the method of DNA comets based on measuring the effect of $C_{60}(OH)_{24}$ on the integrity of the DNA of human peripheral blood mononuclear cells (PBMC) using alkaline gel electrophoresis [51]. The DNA comets were stained with the propidium iodide aqueous solution (C = 10 μg·ml^{-1}) and visualised using the Micromed 3 LUM fluorescence microscope (Russia). The tail lengths were measured using CASP software (version 1.2.2). The DNA content in the tail and the tail length were determined experimentally; the tail moment was calculated as the percentage of DNA in the tail multiplied by the length between the centre of the head and the tail [52].

2.3.13. Computer simulation

MD simulations were performed using GROMACS 5 software suite [53]; the visualisations were made using VMD program [54]. We chose the recent OPLS-AA/M force field [55], which is the well-known OPLS-AA force field with improved protein parameters. The potential model for HSA was obtained according to the protonation states corresponding to pH 7. The models for fullerenol isomers were built following the standard approach in OPLS-AA force field. Namely, at the first step, the quantum-chemical geometry optimisation was performed at RHF/6-31G(d) level of theory. At the second step, the produced distribution of electrostatic potential was fitted with a set of point charges by means of CHelpG algorithm. This procedure was performed for both uniform (random distribution of hydroxyl groups on the fullerene core surface) and “Saturn-like” (across the equatorial region of the fullerene core surface) isomers [38], the R.E.D. server was used to facilitate the task [56]. For the hydroxyl groups,

the atom types of diols were taken (atom types #169, #170). The carbon fullerene atoms were described with the parameters from the work of Girifalco [57], while the rest of sp^2-hybridised atoms were attributed with parameters for alkene C (atom type #141), and sp^3-hybridised atoms were attributed with the atom type #159. The water model was TIP3P; for Na^+ and Cl^- ions, the default parameters were used.

The simulation cells were assembled according to the following procedure. The HSA molecule (in the crystallographic configuration) was solvated in a cubic water box with the side length equal to 10 nm containing ~30,000 water molecules, and the neutralising counter-ions and physiological saline were added resulting in 96 Na^+ and 81 Cl^- ions. Then, the fullerenol molecule was placed at the docking sites DS1, DS2 or DS3 (Fig. 1). The molecule appeared too large to fit in the sites in the initial HSA configuration, therefore an auxiliary simulation was necessary. Specifically, for each isomer in each docking site, a 500 ps slow-growth MD simulation was performed. In the initial state, the interactions between the fullerenol and HSA were zeroed, and they were gradually restored to the normal intensity during the calculation. The fullerenol was restrained in the initial location. As a result, six configurations of the fullerenol–HSA complex were obtained (Fig. 2).

In addition to the above-mentioned configurations with fullerenol placed in the docking sites (DS1, DS2 or DS3), we also prepared two configurations where fullerenol isomers were located on the surface of the protein (Fig. 1) following the same procedure. The first location was called “surface 1” further in the text and it was in a fold of HSA; the second place was called “surface 2” in which the fullerenol only made a contact with HSA. These configurations were taken as initial for the productive MD runs of 20 ns long. The parameters were as follows: T = 298.15 K and p = 1 bar, velocity-rescale thermostat, Parrinello-Rahman barostat, 2 fs time step, PME method for electrostatic interactions, 1 nm cut-off of van der Waals interactions, constraints on all bonds.

2.3. Statistics analysis

All calculations were performed using Origin software (Origin Lab Corporation, Northampton, Massachusetts, USA). P-values were considered significant at 0.05, 0.01, and 0.001. Data were analysed using Student's t-test. Physicochemical experiments were carried out three times. All biological experiments were repeated eight times. All data are presented as mean ± SEM.

3. Results and discussions

3.1. The effect of $C_{60}(OH)_{24}$ on spontaneous erythrocyte haemolysis

To assess the biocompatibility of $C_{60}(OH)_{24}$ its effect on the spontaneous erythrocyte haemolysis was studied. In the case of substances compatible with blood, the erythrocyte membrane remains intact, and the content of the cell are not released. In our case, the toxicity of $C_{60}(OH)_{24}$ was determined by evaluating the released haemoglobin. Fig. 3 shows that $C_{60}(OH)_{24}$, when incubated for 1 and 3 hours, caused a very mild haemolysis in the whole concentration range; the rate of haemolysis was dose- and time-dependent. It is generally accepted that the nanomaterials are classified as non-haemolytic if the haemolysis rate does not exceed 5% [58]. Consequently, fullerenol $C_{60}(OH)_{24}$ can be considered as safe in concentrations up to 100 μM.

3.2. Evaluation of $C_{60}(OH)_{24}$ anti-/pro-oxidant properties

It is known that erythrocyte lysis is initiated by irradiation with ultraviolet or visible light in the presence of photosensitisers, the most effective of which are porphyrins and their derivatives [59], in particular Radachlorin. It was found that the photodynamic effect is primarily due to the generation of singlet oxygen, and other ROS. Binding of porphyrins to cell membranes leads to the decrease of the photostability of membranes [7].

Fig. 4 shows the dependence of TC_{50} on the concentration of $C_{60}(OH)_{24}$. As can be seen from the obtained results, $C_{60}(OH)_{24}$ was statistically significantly, in comparison with the

control, inhibited haemolysis induced by Radachlorin, which was manifested in the increase of the haemolysis time of 50 % of erythrocytes (TC_{50}). It can be concluded that $C_{60}(OH)_{24}$ exhibits dose-dependent antioxidant activity.

3.3. Effect of $C_{60}(OH)_{24}$ on coagulation haemostasis

As can be seen from the data presented in Table 3, $C_{60}(OH)_{24}$ at the concentrations of 50–100 μM leads to a statistically significant increase in PT and TT in the blood of healthy donors compared to the control. An increase in aPTT is observed at all studied concentrations of the fullerenol. Thus, $C_{60}(OH)_{24}$ exhibits pronounced anticoagulant properties in the studied concentration range (C = 10–100 μM).

3.4. NO-radical uptake

NO-radical is an important chemical mediator generated by endothelial cells, macrophages, neurons and involved in the regulation of various physiological processes. Excess concentration of NO-radical uptake provokes cytotoxic effects during various disorders such as AIDS, cancer, Alzheimer's disease, and arthritis. The oxygen reacts with the excess of NO-radical uptake to generate nitrite and peroxynitrite anions, which act as free radicals.

From Fig. 5 it can be seen that fullerenol reacts with the NO-radical in the entire concentration range (C = 10–200 μM), although its antiradical activity is less pronounced compared to sodium azide. We can conclude that fullerenol is a weak NO-radical scavenger, and it is impossible to evaluate the IC_{50}. At the same time, previously we obtained experimental data on the kinetics of the interaction of $C_{60}(OH)_{22–24}$ with DPPH radical and determined moderate antiradical activity of fullerenol [40]. The results obtained are in good agreement with previously published work on the antioxidant properties of polyhydroxylated fullerenes with various content of hydroxyl groups [60–63].

3.5. Reducing capacity of $C_{60}(OH)_{24}$

It can be seen from the graph presented in Fig. 6 that fullerenol exhibits the properties of a reducing agent in the entire concentration range (C = 500–1100 μM), although the reducing capacity is less pronounced compared to ascorbic acid. The reducing capacity of fullerenol is dose dependent. Fe^{3+} reduction is often used as an indicator of the electron donating activity, which is potentially important for determining the fullerenol action mechanism. The reducing capacity is associated with the antioxidant potential of fullerenol. In our case, the results of NO-radical uptake and reducing capacity methods are in good agreement: fullerenol possesses low antiradical activity against NO-radicals and at the same time a moderate activity in the electron donating reaction with Fe^{3+}. Thus, the results obtained are in good agreement with the data of ref. [9].

3.6. Photobleaching

The photosensitiser degradation was evaluated by measuring the photodegradation rate constants, the values of which were determined as the slope of the kinetic curves in the coordinates $\ln(A_t / A_0) - t$. The decrease in k_{deg} indicates the presence of singlet oxygen quencher properties of the test compound. In turn, the increase in k_{deg} indicates that the test compound has the properties of a singlet oxygen inducer.

Radachlorin absorption spectra were measured in the absence and in the presence of various concentrations of $C_{60}(OH)_{24}$ (C = 10, 50, 75, 100 μM). The solution of sodium azide (C = 500 μM), which is a strong antioxidant, was used as a control. As an example, the absorption spectra of Radachlorin in the presence of $C_{60}(OH)_{24}$ (C = 2.5 mg·l^{-1}), in the absence, and under irradiation (10–50 s) are shown in Fig. 7. Based on the obtained spectra with various fullerenol content, the dependences of $\ln(A_t / A_0)$ on the irradiation time were plotted. Fig. 8 and Table 4 reveal that the addition of $C_{60}(OH)_{24}$ to Radachlorin leads to the decrease in k_{deg}. Thus, it can be stated that $C_{60}(OH)_{24}$ exhibits dose-dependent antioxidant properties.

3.7. Human platelet aggregation

Table 5 shows the results of measuring the effect of $C_{60}(OH)_{24}$ on human platelet aggregation in the presence of the platelet aggregation inducer (ADP). It can be concluded that $C_{60}(OH)_{24}$ in the concentration range C = 10–50 μM does not affect platelet aggregation; further increase in the concentration of $C_{60}(OH)_{24}$ leads to the decrease in aggregation compared to the control group. Thus, $C_{60}(OH)_{24}$ has antiplatelet activity at C > 50 μM in tests for ADP-induced platelet aggregation.

3.8. Binding of $C_{60}(OH)_{24}$ to HSA by spectrofluorimetric data

Albumin has three main ligand binding sites: (*i*) site I, located in the subdomain IIA (warfarin binding site); (*ii*) site II, located in the subdomain IIIA (ibuprofen binding site); (*iii*) site II located in the subdomain IB (digitonin binding site) [64]. To identify the binding sites of $C_{60}(OH)_{24}$ to HSA, competitive binding experiments were performed in the presence of binding site markers. To determine the binding constants (K_b), as well as the stoichiometry of the binding reaction (n), the Scatchard equation was used:

$$\lg\frac{F_0 - F}{F} = \lg K_b + n\lg Q \qquad (2),$$

where F_0 is the HSA fluorescence intensity in the absence of $C_{60}(OH)_{24}$, F is the HSA fluorescence intensity in the presence of $C_{60}(OH)_{24}$, Q is the molar concentration of $C_{60}(OH)_{24}$.

It is important to take into account the inner-filter effect resulting in the additional quenching of fluorescence caused by the absorption of excitation and emission radiation. This phenomenon may not be considered in our system due to low absorbance.

Fig. 9 presents data on the binding of HSA to $C_{60}(OH)_{24}$ in Hill coordinates ($\lg\frac{F_0 - F}{F}$ *vs* $\lg Q$). The obtained dependence has an inflection point, which corresponds to the presence of two binding sites [65]. In the concentration range $C = 3\cdot10^{-7}$–$1.5\cdot10^{-6}$ M, binding to the first site occurs, and in the concentration range $C = 6.0\cdot10^{-6}$–$2.4\cdot10^{-5}$ M binding to the second one takes place. In Table S1 (Supporting Information), the data on the binding of HSA to $C_{60}(OH)_{24}$

with markers (warfarin, ibuprofen, digitonin) are presented in Hill coordinates. Table 6 demonstrates the data on the stoichiometry of the binding of HSA to $C_{60}(OH)_{24}$ (n), as well as the logarithm of the binding constants in the presence and in the absence of markers (warfarin, ibuprofen, digitonin) for two concentration ranges $C = 3 \cdot 10^{-7}$–$1.5 \cdot 10^{-6}$ M and $C = 6.0 \cdot 10^{-6}$–$2.4 \cdot 10^{-5}$ M.

From the obtained data, it is seen that (*i*) the values of $\lg K_b$ and n do not change in both concentration ranges with the addition of warfarin; (*ii*) in the concentration range $C = 3 \cdot 10^{-7}$–$1.5 \cdot 10^{-6}$ M, the decrease in $\lg K_b$ and n is observed with the addition of digitonin; (*iii*) in the concentration range $C = 6.0 \cdot 10^{-6}$–$2.4 \cdot 10^{-5}$ M, the decrease in $\lg K_b$ and n is observed with the addition of ibuprofen. Based on the values of the binding constants ($K_b = 2.51 \pm 0.09 \cdot 10^5$ M^{-1} for the first concentration site and $7.9 \pm 0.5 \cdot 10^2$ M^{-1} for the second one), $C_{60}(OH)_{24}$ forms a strong complex with HSA in the subdomain IB and it weakly binds in the subdomain IIIA.

3.9. Binding to HSA by TSA data

To determine the dissociation constants, we applied an approach described in refs. [49,50]. The experimental data on the fluorescence vs temperature (*a*) and its first derivative (*b*) are presented in Fig. 10. The obtained results on HSA melting point vs fullerenol concentration are demonstrated in Fig. 11. The concentration dependence of the melting point can be clearly divided into two parts: the concentration ranges $C = 0$–$1.6 \cdot 10^{-6}$ M and $C = 3.13 \cdot 10^{-6}$–10^{-4} M corresponding to the digitonin and ibuprofen binding sites of HSA (see Section 3.8). To obtain the values of the dissociation constants for both concentration ranges, the data were processed using the following equation:

$$t = \frac{B_{max} \cdot C}{K_d + C} + NS \cdot C + B \quad (3),$$

where t is the melting point of the $C_{60}(OH)_{24}$–HSA complex, B_{max} is maximum binding (units of temperature), C is the fullerenol concentration, K_d is the dissociation constant (units of concentration), NS is the slope of a non-linear regression (units of temperature divided by units

of concentration), *B* is the measured binding with no ligand added. The correlation parameters are shown in Table 7.

As the result (Fig. 12), the following values of the binding constants (reciprocals of the dissociation constants) were retrieved: $2.28 \cdot 10^5 \pm 0.07$ M^{-1} (C = 0–$1.6 \cdot 10^{-6}$ M) and $4.56 \cdot 10^2 \pm 0.03$ M^{-1} (C = $3.13 \cdot 10^{-6}$–10^{-4} M), which is in good correspondence with the data obtained by spectrofluorimetry.

3.10. Esterase activity

To determine the rate constant of the NPA hydrolysis reaction, the first order reaction equation was used:

$$\ln\left(1-\frac{A_t - A_0}{A_{NF}}\right) = -kt \quad (4),$$

where A_{NF} = 1.86 (the optical density of the nitrophenol solution with 100 μM concentration); A_t is the optical density of the reaction mixture at time t; A_0 is the optical density of the reaction mixture at the initial time; k is the reaction rate constant (min^{-1}); t is the time from the beginning of the reaction (min).

The kinetic dependences of the reaction of NPA hydrolysis with HSA in the absence and in the presence of $C_{60}(OH)_{24}$ were obtained. As an example, Fig. 13 shows the kinetic dependences of the reaction of NPA hydrolysis with HSA in the absence and in the presence of 24 μM $C_{60}(OH)_{24}$.

Further, based on the data on the change in optical density, the dependences were plotted in the coordinates $\ln\left(1-\frac{A_t - A_0}{A_{NF}}\right)$ *vs t*. As an example, Fig. 14 presents the data for the hydrolysis reaction of NPA with HSA in the absence and in the presence of 24 μM $C_{60}(OH)_{24}$.

The first-order reaction rate constants were determined as the slope of the dependence of $\ln\left(1-\frac{A_t-A_0}{A_{NF}}\right)$ on t (Fig. 15). From Fig. 15, it can be seen that $C_{60}(OH)_{24}$ in the concentration range 2.4–24 μM partially inhibits the esterase activity of HSA.

3.11. $C_{60}(OH)_{24}$ binding to DNA

Fig. 16 demonstrates the DNA fluorescence spectra in the absence and in the presence of $C_{60}(OH)_{24}$ at 298.15 K. To determine the binding constants (K_b), as well as the stoichiometry of the binding reaction (n), the Scatchard equation was used (see Eq. 2). For this, the experimental dependences were plotted in Hill coordinates. Fig. 17 shows an example of the dependence in Hill coordinates at 303.15 K. The calculated values of K_b and n are presented in Table 8. The order of the obtained K_b values in the temperature range T = 303.15–318.15 K (10^3–10^4 M^{-1}) indicates the formation of strong $C_{60}(OH)_{24}$ complexes with DNA. The changes in the enthalpy and entropy of the reaction of $C_{60}(OH)_{24}$ binding to DNA were calculate using the van't Hoff equation neglecting the influence of temperature:

$$\ln K_b = -\frac{\Delta H}{RT} + \frac{\Delta S}{R} \quad (5),$$

where ΔH and ΔS are the changes in the enthalpy and the entropy of the reactions of $C_{60}(OH)_{24}$ binding to DNA, R is the gas constant, T is the absolute temperature.

The changes in the Gibbs energy (ΔG) of the reaction of $C_{60}(OH)_{24}$ binding to DNA in the temperature range 303.15–318.15 K was calculated using the following equation:

$$\Delta G = \Delta H - T\Delta S \quad (6).$$

Negative ΔG values in the temperature range 303.15–318.15 K indicate that the binding process of the $C_{60}(OH)_{24}$ derivative to DNA is thermodynamically favourable. Positive values of ΔH and ΔS are typical to hydrophobic interactions, therefore, it can be assumed that the formation of $C_{60}(OH)_{24}$ complexes with DNA occurs due to the fullerene core. In ref. [66], the authors showed that fullerenol $C_{60}(OH)_{24}$ interacts with the phosphate backbone of the outer

side of the native DNA double helix, as well as with pairs of nitrogenous bases inside the major groove of DNA. Comparison of K_b shows that the values obtained in [66] exceed the K_b values obtained in this study by one to two orders of magnitude. This fact is due to the different temperature ranges in which the binding study was carried out, as well as to the fact that different methods were used to obtain fullerenols and, as a consequence, the synthesised adducts had different compositions. For example, it was shown by solid-state ^{13}C NMR spectroscopy that the fullerenol used in our study contains a small amount of epoxy groups.

3.12. Genotoxicity results

The average values of % tail DNA, the tail length and the tail moment of comets observed for human PBMCs incubated in the presence of H_2O_2 (positive control), phosphate-saline buffer (negative control) and $C_{60}(OH)_{24}$ are presented in Table 9. It can be seen that the amount of DNA damage in the presence of H_2O_2 is significantly higher than that of control cells. As an example, Fig. 18 presents the photographs of the DNA comets in the presence of H_2O_2 (C = 3.4 μg·l^{-1}), the phosphate-saline buffer, and $C_{60}(OH)_{24}$ (C = 10, 50, 75, and 100 μM). It can be concluded that $C_{60}(OH)_{24}$ possesses moderate dose dependent genotoxicity. Based on the study of the frequencies of micronucleus formation and chromosomal aberrations, the authors of refs [20,67] showed that fullerenol $C_{60}(OH)_{24}$ does not cause significant genotoxic effects to CHO-K1 cells (Chinese hamster ovary cells K1) and human peripheral blood monocytes, and also established its projective effect when cells are exposed to the alkylating agent Mitomycin C.

3.13. Computer simulation

The analysis of the MD simulation results showed that both uniform and Saturn-like isomers are strongly bound in the docking sites. During the 20 ns of simulations, the molecules remained in the initial locations or close to them (Fig. 2). This can be explained by the buried location of the molecule, which demands considerable deformation of the protein for the

fullerenol to desorb, and the presence of hydrogen bonds between the constituents. The average number of hydrogen bonds is listed in Table 10, and the time evolution is depicted in Fig. 19. The isomers show similar behaviour except for the DS2 site where the Saturn-like isomer forms approximately two times more hydrogen bonds with HSA.

The results of the simulations started from the initial configurations with fullerenol located near the HSA surface shed more light on the importance of the $C_{60}(OH)_{24}$–HSA hydrogen bonding. In the case when the fullerenol molecule was placed in a fold ("surface 1"), it remained in that place being hold by hydrogen bonds. On the contrary, when the uniform isomer was placed at the other location ("surface 2") that did not provide sufficient hydrogen bonding, it desorbed and remained in the solution except at the interval (12–20 ns) when it was adsorbed on the surface being bound with 2.7 hydrogen bonds in average. The Saturn-like isomer in the same position ("surface 2") managed to form more hydrogen bonds with the surface (~3.6), which allowed it to stay near the initial position during all 20 ns of the calculations. This indicates that for strong binding, abundant hydrogen bonding with HSA is needed. Also, the binding is seen to occur not only in the specific docking sites, but on the surface, as well.

Finally, examining the initial configurations makes it clear that at experimental conditions, the fullerenol molecules are unable to reach the DS1 site compared to more reachable DS2 and DS3 sites.

4. Conclusions

We present the experimental data on the biocompatibility of aqueous solutions of well-defined fullerenol $C_{60}(OH)_{24}$, namely, its cyto- and genotoxicity, spontaneous and photo-induced haemolysis, photobleaching, platelet aggregation, binding to HSA and DNA. We found that $C_{60}(OH)_{24}$ has low geno- and cytotoxicity, and it exhibits anti-aggregative and antioxidant properties. The study of $C_{60}(OH)_{24}$ binding to HSA demonstrated that the

interaction of the fullerenol with HSA occurs through the subdomains IB (digitonin binding site) and IIIA (ibuprofen binding site); the obtained values of the binding constants indicate that HSA can perform transport functions in the bloodstream. We conclude that $C_{60}(OH)_{24}$ is a promising compound for nanomedicine as a basis for the synthesis of new biomedical materials, as well as due to its pronounced antioxidant properties. The work showed its high biocompatibility. $C_{60}(OH)_{24}$ also demonstrates increased anticoagulant properties which make this material promising as a nano-modifier for the development of heart valves and vascular stents.

Acknowledgements

The work was supported by a grant from the Russian Science Foundation (20-79-10064). Research was performed using the equipment of the Resource Centre "GeoModel", Centre for Chemical Analysis and Materials Research, Interdisciplinary Resource Centre for Nanotechnology, Centre for Diagnostics of Functional Materials for Medicine, Pharmacology and Nanoelectronics, Magnetic Resonance Research Centre, Centre for Physical Methods of Surface Investigation, Thermogravimetric and Calorimetric Research Centre; computational resources provided by Computer Centre of SPbU of the Research Park of Saint Petersburg State University.

Supporting information description

Intermediate calculation of $C_{60}(OH)_{24}$–HSA binding data.

References

(1) Cataldo, F.; Da Ros, T. *Medicinal Chemistry and Pharmacological Potential of Fullerenes and Carbon Nanotubes*; Carbon Materials: Chemistry and Physics; Springer Netherlands: Dordrecht, 2008; Vol. 1. https://doi.org/10.1007/978-1-4020-6845-4.

(2) Piotrovsky, L. B.; Kiselev, O. I. *Fullerenes in Biology*; Rostok: Saint Petersburg, 2006.

(3) Semenov, K. N.; Charykov, N. A.; Postnov, V. N.; Sharoyko, V. V.; Vorotyntsev, I. V.; Galagudza, M. M.; Murin, I. V. Fullerenols: Physicochemical Properties and Applications. *Prog. Solid State Chem.* **2016**, *44* (2), 59–74. https://doi.org/10.1016/j.progsolidstchem.2016.04.002.

(4) Sforzini, S.; Oliveri, C.; Barranger, A.; Jha, A. N.; Banni, M.; Moore, M. N.; Viarengo, A. Effects of Fullerene C_{60} in Blue Mussels: Role of MTOR in Autophagy Related Cellular/Tissue Alterations. *Chemosphere* **2020**, *246*. https://doi.org/10.1016/j.chemosphere.2019.125707.

(5) Lichota, A.; Piwoński, I.; Michlewska, S.; Krokosz, A. A Multiparametric Study of Internalization of Fullerenol $C_{60}(OH)_{36}$ Nanoparticles into Peripheral Blood Mononuclear Cells: Cytotoxicity in Oxidative Stress Induced by Ionizing Radiation. *Int. J. Mol. Sci.* **2020**, *21* (7). https://doi.org/10.3390/ijms21072281.

(6) Krokosz, A.; Grebowski, J.; Rodacka, A.; Pasternak, B.; Puchala, M. The Effect of Fullerenol $C_{60}(OH)_{\sim 30}$ on the Alcohol Dehydrogenase Activity Irradiated with X-Rays. *Radiat. Phys. Chem.* **2014**, *97*, 102–106. https://doi.org/10.1016/j.radphyschem.2013.11.009.

(7) Eropkin, M. Y.; Melenevskaya, E. Y.; Nasonova, K. V.; Bryazzhikova, T. S.; Eropkina, E. M.; Danilenko, D. M.; Kiselev, O. I. Synthesis and Biological Activity of Fullerenols with Various Contents of Hydroxyl Groups. *Pharm. Chem. J.* **2013**, *47* (2), 87–91. https://doi.org/10.1007/s11094-013-0901-x.

(8) Yin, J.-J.; Lao, F.; Fu, P. P.; Wamer, W. G.; Zhao, Y.; Wang, P. C.; Qiu, Y.; Sun, B.; Xing, G.; Dong, J. et al. The Scavenging of Reactive Oxygen Species and the Potential for Cell Protection by Functionalized Fullerene Materials. *Biomaterials* **2009**, *30* (4), 611–621. https://doi.org/10.1016/j.biomaterials.2008.09.061.

(9) Mirkov, S. M.; Djordjevic, A. N.; Andric, N. L.; Andric, S. A.; Kostic, T. S.; Bogdanovic, G. M.; Vojinovic-Miloradov, M. B.; Kovacevic, R. Z. Nitric Oxide-Scavenging Activity of Polyhydroxylated Fullerenol, $C_{60}(OH)_{24}$. *Nitric Oxide* **2004**, *11* (2), 201–207. https://doi.org/10.1016/j.niox.2004.08.003.

(10) Saitoh, Y.; Miyanishi, A.; Mizuno, H.; Kato, S.; Aoshima, H.; Kokubo, K.; Miwa, N. Super-Highly Hydroxylated Fullerene Derivative Protects Human Keratinocytes from UV-Induced Cell Injuries Together with the Decreases in Intracellular ROS Generation and DNA Damages. *J. Photochem. Photobiol. B Biol.* **2011**, *102* (1), 69–76. https://doi.org/10.1016/j.jphotobiol.2010.09.006.

(11) Jiao, F.; Liu, Y.; Qu, Y.; Li, W.; Zhou, G.; Ge, C.; Li, Y.; Sun, B.; Chen, C. Studies on Anti-Tumor and Antimetastatic Activities of Fullerenol in a Mouse Breast Cancer Model. *Carbon N. Y.* **2010**, *48* (8), 2231–2243. https://doi.org/10.1016/j.carbon.2010.02.032.

(12) Ma, H.; Zhao, J.; Meng, H.; Hu, D.; Zhou, Y.; Zhang, X.; Wang, C.; Li, J.; Yuan, J.; Wei, Y. Carnosine-Modified Fullerene as a Highly Enhanced ROS Scavenger for Mitigating Acute Oxidative Stress. *ACS Appl. Mater. Interfaces* **2020**, *12* (14), 16104–16113. https://doi.org/10.1021/acsami.0c01669.

(13) Đurašević, S.; Nikolić, G.; Todorović, A.; Drakulić, D.; Pejić, S.; Martinović, V.; Mitić-Ćulafić, D.; Milić, D.; Kop, T. J.; Jasnić, N. et al. Effects of Fullerene C_{60} Supplementation on Gut Microbiota and Glucose and Lipid Homeostasis in Rats. *Food Chem. Toxicol.* **2020**, *140*. https://doi.org/10.1016/j.fct.2020.111302.

(14) Thong, N. M.; Vo, Q. V.; Le Huyen, T.; Van Bay, M.; Dung, N. N.; Thu Thao, P. T.; Nam, P. C. Functionalization and Antioxidant Activity of Polyaniline-Fullerene Hybrid Nanomaterials: A Theoretical Investigation. *RSC Adv.* **2020**, *10* (25), 14595–14605. https://doi.org/10.1039/d0ra00903b.

(15) Gudkov, S. V.; Guryev, E. L.; Gapeyev, A. B.; Sharapov, M. G.; Bunkin, N. F.; Shkirin, A. V.; Zabelina, T. S.; Glinushkin, A. P.; Sevost'yanov, M. A.; Belosludtsev, K. N. et al. Unmodified Hydrated C_{60} Fullerene Molecules Exhibit Antioxidant Properties, Prevent Damage to DNA and Proteins Induced by Reactive Oxygen Species and Protect Mice against Injuries Caused by Radiation-Induced Oxidative Stress. *Nanomedicine Nanotechnology, Biol. Med.* **2019**, *15* (1), 37–46. https://doi.org/10.1016/j.nano.2018.09.001.

(16) Krokosz, A.; Lichota, A.; Nowak, K. E.; Grebowski, J. Carbon Nanoparticles as Possible Radioprotectors in Biological Systems. *Radiat. Phys. Chem.* **2016**, *128*, 143–150. https://doi.org/10.1016/j.radphyschem.2016.07.006.

(17) Jović, D. S.; Seke, M. N.; Djordjevic, A. N.; Mrdanović, J.; Aleksić, L. D.; Bogdanović, G. M.; Pavić, A. B.; Plavec, J. Fullerenol Nanoparticles as a New Delivery System for Doxorubicin. *RSC Adv.* **2016**, *6* (45), 38563–38578. https://doi.org/10.1039/c6ra03879d.

(18) Tao, R.; Wang, C.; Lu, Y.; Zhang, C.; Zhou, H.; Chen, H.; Li, W. Characterization and Cytotoxicity of Polyprenol Lipid and Vitamin E-TPGS Hybrid Nanoparticles for Betulinic Acid and Low-Substituted Hydroxyl Fullerenol in MHCC97H and L02 Cells. *Int. J. Nanomedicine* **2020**, *15*, 2733–2749. https://doi.org/10.2147/IJN.S249773.

(19) Çavaş, T.; Çinkiliç, N.; Vatan, O.; Yilmaz, D. Effects of Fullerenol Nanoparticles on Acetamiprid Induced Cytoxicity and Genotoxicity in Cultured Human Lung Fibroblasts. *Pestic. Biochem. Physiol.* **2014**, *114* (1), 1–7.

https://doi.org/10.1016/j.pestbp.2014.07.008.

(20) Mrbanovic, Ž. J.; Šolajic, S. V.; Bogdanović, V. V.; Djordjevic, A. N.; Bogdanović, G. M.; Injac, R. D.; Rakočević, Z. L. J. Effects of Fullerenol Nano Particles $C_{60}(OH)_{24}$ on Micronuclei and Chromosomal Aberrations' Frequency in Peripheral Blood Lymphocytes. *Dig. J. Nanomater. Biostructures* **2012**, *7* (2), 673–686.

(21) Bogdanović, V.; Slavić, M.; Mrdanović, J.; Šolajić, S.; Djordjević, A. The Activity of Superoxide-Dismutase in Animal Cell Culture CHO-K1 after Treatment with Fullerenol and Mytomicine C. *Hem. Ind.* **2009**, *63* (3), 143–149. https://doi.org/10.2298/HEMIND0903143B.

(22) Wang, Z.; Wang, S.; Lu, Z.; Gao, X. Syntheses, Structures and Antioxidant Activities of Fullerenols: Knowledge Learned at the Atomistic Level. *Journal of Cluster Science*. Springer New York LLC February 2015, pp 375–388. https://doi.org/10.1007/s10876-015-0855-0.

(23) Torres, V. M.; Srdjenovic, B.; Jacevic, V.; Simic, V. D.; Djordjevic, A.; Simplício, A. L. Fullerenol $C_{60}(OH)_{24}$ Prevents Doxorubicin-Induced Acute Cardiotoxicity in Rats. *Pharmacol. Rep.* **2010**, *62* (4), 707–718. https://doi.org/10.1016/s1734-1140(10)70328-5.

(24) Chaudhuri, P.; Paraskar, A.; Soni, S.; Mashelkar, R. A.; Sengupta, S. Fullerenol−cytotoxic Conjugates for Cancer Chemotherapy. *ACS Nano* **2009**, *3* (9), 2505–2514. https://doi.org/10.1021/nn900318y.

(25) Grebinyk, A.; Prylutska, S.; Grebinyk, S.; Prylutskyy, Y.; Ritter, U.; Matyshevska, O.; Dandekar, T.; Frohme, M. Complexation with C_{60} Fullerene Increases Doxorubicin Efficiency against Leukemic Cells In Vitro. *Nanoscale Res. Lett.* **2019**, *14* (1), 61. https://doi.org/10.1186/s11671-019-2894-1.

(26) Chueh, S. C.; Lai, M. K.; Chen, S. C.; Chiang, L. Y.; Chen, W. C. Fullerenols in Canine

Renal Preservation—A Preliminary Report. *Transplant. Proc.* **1997**, *29* (1–2), 1313–1315. https://doi.org/10.1016/S0041-1345(96)00572-6.

(27) Lai, H. S.; Chen, Y.; Chen, W. J.; Chang, J.; Chiang, L. Y. Free Radical Scavenging Activity of Fullerenol on Grafts after Small Bowel Transplantation in Dogs. *Transplant. Proc.* **2000**, *32* (6), 1272–1274.

(28) Ye, S.; Chen, M.; Jiang, Y.; Chen, M.; Wang, Y.; Hou, Z.; Ren, L.; Zhou, T. Polyhydroxylated Fullerene Attenuates Oxidative Stress-Induced Apoptosis via a Fortifying Nrf2-Regulated Cellular Antioxidant Defence System. *Int. J. Nanomedicine* **2014**, 2073. https://doi.org/10.2147/IJN.S56973.

(29) Kamat, J. P.; Devasagayam, T. P. A.; Mohan, H.; Chiang, L. Y.; Mittal, J. P. Effect of $C_{60}(OH)_{18}$ on Membranes of Rat Liver Microsomes during Photosensitization. *Fuller. Sci. Technol.* **1998**, *6* (4), 663–679. https://doi.org/10.1080/10641229809350227.

(30) Injac, R.; Perse, M.; Obermajer, N.; Djordjevic-Milic, V.; Prijatelj, M.; Djordjevic, A.; Cerar, A.; Strukelj, B. Potential Hepatoprotective Effects of Fullerenol $C_{60}(OH)_{24}$ in Doxorubicin-Induced Hepatotoxicity in Rats with Mammary Carcinomas. *Biomaterials* **2008**, *29* (24–25), 3451–3460. https://doi.org/10.1016/j.biomaterials.2008.04.048.

(31) Xu, J.-Y.; Su, Y.-Y.; Cheng, J.-S.; Li, S.-X.; Liu, R.; Li, W.-X.; Xu, G.-T.; Li, Q.-N. Protective Effects of Fullerenol on Carbon Tetrachloride-Induced Acute Hepatotoxicity and Nephrotoxicity in Rats. *Carbon N. Y.* **2010**, *48* (5), 1388–1396. https://doi.org/10.1016/j.carbon.2009.12.029.

(32) Panova, G. G.; Semenov, K. N.; Shilova, O. A.; Khomyakov, Y. V.; Anikina, L. M.; Charikov, N. A.; Artemjeva, A. M.; Kanash, E. V.; Khamova, T. B.; Udalova, O. R. Water-Soluble Derivatives of Fullerenes and Silicon-Containing Sol-Nanocomposites as the Promising Nanomaterials for Crop Production. *Agrophysica* **2015**, *4*, 37–48.

(33) Bityutskii, N. P.; Yakkonen, K. L.; Lukina, K. A.; Semenov, K. N. Fullerenol Increases

Effectiveness of Foliar Iron Fertilization in Iron-Deficient Cucumber. *PLoS One* **2020**, *15* (5), e0232765. https://doi.org/10.1371/journal.pone.0232765.

(34) Semenov, K. N.; Andrusenko, E. V.; Charykov, N. A.; Litasova, E. V.; Panova, G. G.; Penkova, A. V.; Murin, I. V.; Piotrovskiy, L. B. Carboxylated Fullerenes: Physico-Chemical Properties and Potential Applications. *Prog. Solid State Chem.* **2017**, *47–48*, 19–36. https://doi.org/10.1016/j.progsolidstchem.2017.09.001.

(35) Pochkaeva, E. I.; Podolskiy, N. E.; Zakusilo, D. N.; Petrov, A. V.; Charykov, N. A.; Vlasov, T. D.; Penkova, A. V.; Vasina, L. V.; Murin, I. V.; Sharoyko, V. V. et al. Fullerene Derivatives with Amino Acids, Peptides and Proteins: From Synthesis to Biomedical Application. *Prog. Solid State Chem.* **2020**, 100255. https://doi.org/10.1016/j.progsolidstchem.2019.100255.

(36) Sharoyko, V. V.; Ageev, S. V.; Podolsky, N. E.; Petrov, A. V.; Litasova, E. V.; Vlasov, T. D.; Vasina, L. V.; Murin, I. V.; Piotrovskiy, L. B.; Semenov, K. N. Biologically Active Water-Soluble Fullerene Adducts: Das Glasperlenspiel (by H. Hesse)? *J. Mol. Liq.* **2021**, *323*, 114990. https://doi.org/10.1016/j.molliq.2020.114990.

(37) Sharoyko, V. V.; Ageev, S. V.; Meshcheriakov, A. A.; Akentiev, A. V.; Noskov, B. A.; Rakipov, I. T.; Charykov, N. A.; Kulenova, N. A.; Shaimardanova, B. K.; Podolsky, N. E. et al. Physicochemical Study of Water-Soluble $C_{60}(OH)_{24}$ Fullerenol. *J. Mol. Liq.* **2020**, *311*, 113360. https://doi.org/10.1016/j.molliq.2020.113360.

(38) Markin, A. V.; Samosudova, Y. S.; Ogurtsov, T. G.; Smirnova, N. N.; Ageev, S. V.; Podolsky, N. E.; Petrov, A. V.; Murin, I. V.; Semenov, K. N. Heat Capacity and Standard Thermodynamic Functions of the Fullerenol $C_{60}(OH)_{24}$. *J. Chem. Thermodyn.* **2020**, *149*, 106192. https://doi.org/10.1016/j.jct.2020.106192.

(39) Djordjević, A.; Vojinović-Miloradov, M.; Petranović, N.; Devečerski, A.; Lazar, D.; Ribar, B. Catalytic Preparation and Characterization of $C_{60}Br_{24}$. *Fuller. Sci. Technol.*

1998, *6* (4), 689–694. https://doi.org/10.1080/10641229809350229.

(40) Podolsky, N. E.; Marcos, M. A.; Cabaleiro, D.; Semenov, K. N.; Lugo, L.; Petrov, A. V.; Charykov, N. A.; Sharoyko, V. V.; Vlasov, T. D.; Murin, I. V. Physico-Chemical Properties of $C_{60}(OH)_{22–24}$ Water Solutions: Density, Viscosity, Refraction Index, Isobaric Heat Capacity and Antioxidant Activity. *J. Mol. Liq.* **2019**, *278*, 342–355. https://doi.org/10.1016/j.molliq.2018.12.148.

(41) Semenov, K. N.; Charykov, N. A.; Keskinov, V. N. Fullerenol Synthesis and Identification. Properties of the Fullerenol Water Solutions. *J. Chem. Eng. Data* **2011**, *56* (2), 230–239. https://doi.org/10.1021/je100755v.

(42) Vlakh, E. G.; Grachova, E. V.; Zhukovsky, D. D.; Hubina, A. V.; Mikhailova, A. S.; Shakirova, J. R.; Sharoyko, V. V.; Tunik, S. P.; Tennikova, T. B. Self-Assemble Nanoparticles Based on Polypeptides Containing C-Terminal Luminescent Pt-Cysteine Complex. *Sci. Rep.* **2017**, *7*, 41991. https://doi.org/10.1038/srep41991.

(43) Galebskaya L. V.; Solovtsova I. L.; Mikhailova I. A. Device for the Study of Photoinduced Cytolysis. RU114157U1, 2012.

(44) Galebskaya, L. V.; Solovtsova, I. L.; Miroshnikova, E. B.; Mikhailova, I. A.; Sushkin, M. E.; Razumny, A. V.; Babina, A. V.; Fomina, V. A. The Importance of a Photosensitizer Bleaching Registration for the Evaluation of Mechanism of Preparation Action on the Photo-Induced Hemolysis. *Biomed. Photonics* **2017**, *6* (3), 33–38. https://doi.org/10.24931/2413-9432-2017-6-3-33-38.

(45) Mandal, S.; Hazra, B.; Sarkar, R.; Biswas, S.; Mandal, N. Assessment of the Antioxidant and Reactive Oxygen Species Scavenging Activity of Methanolic Extract of Caesalpinia Crista Leaf. *Evidence-based Complement. Altern. Med.* **2011**, *2011*, 173768. https://doi.org/10.1093/ecam/nep072.

(46) Oyaizu, M. Studies on Products of Browning Reaction. Antioxidative Activities of

Products of Browning Reaction Prepared from Glucosamine. *Japanese J. Nutr. Diet.* **1986**, *44* (6), 307–315. https://doi.org/10.5264/eiyogakuzashi.44.307.

(47) Bursal, E.; Köksal, E. Evaluation of Reducing Power and Radical Scavenging Activities of Water and Ethanol Extracts from Sumac (Rhus Coriaria L.). *Food Res. Int.* **2011**, *44* (7), 2217–2221. https://doi.org/10.1016/j.foodres.2010.11.001.

(48) Hadjur, C.; Lange, N.; Rebstein, J.; Monnier, P.; van den Bergh, H.; Wagnières, G. Spectroscopic Studies of Photobleaching and Photoproduct Formation of Meta(Tetrahydroxyphenyl)Chlorin (m-THPC) Used in Photodynamic Therapy. The Production of Singlet Oxygen by m-THPC. *J. Photochem. Photobiol. B Biol.* **1998**, *45* (2–3), 170–178. https://doi.org/10.1016/S1011-1344(98)00177-8.

(49) Keeffe, J. *ThermoFluor Assay Protocol*; 2013.

(50) Vivoli, M.; Novak, H. R.; Littlechild, J. A.; Harmer, N. J. Determination of Protein-Ligand Interactions Using Differential Scanning Fluorimetry. *J. Vis. Exp.* **2014**, No. 91, 51809. https://doi.org/10.3791/51809.

(51) Gaponenko, I. N.; Ageev, S. V.; Iurev, G. O.; Shemchuk, O. S.; Meshcheriakov, A. A.; Petrov, A. V.; Solovtsova, I. L.; Vasina, L. V.; Tennikova, T. B.; Murin, I. V. et al. Biological Evaluation and Molecular Dynamics Simulation of Water-Soluble Fullerene Derivative $C_{60}[C(COOH)_2]_3$. *Toxicol. Vitr.* **2020**, *62*, 104683. https://doi.org/10.1016/j.tiv.2019.104683.

(52) Olive, P. L.; Banáth, J. P.; Durand, R. E. Heterogeneity in Radiation-Induced DNA Damage and Repair in Tumor and Normal Cells Measured Using the “Comet” Assay. *Radiat. Res.* **1990**, *122* (1), 86–94. https://doi.org/10.2307/3577587.

(53) Abraham, M. J.; Murtola, T.; Schulz, R.; Páll, S.; Smith, J. C.; Hess, B.; Lindah, E. GROMACS: High Performance Molecular Simulations through Multi-Level Parallelism from Laptops to Supercomputers. *SoftwareX* **2015**, *1–2*, 19–25.

https://doi.org/10.1016/j.softx.2015.06.001.

(54) Humphrey, W.; Dalke, A.; Schulten, K. VMD: Visual Molecular Dynamics. *J. Mol. Graph.* **1996**, *14* (1), 33–38. https://doi.org/10.1016/0263-7855(96)00018-5.

(55) Robertson, M. J.; Tirado-Rives, J.; Jorgensen, W. L. Improved Peptide and Protein Torsional Energetics with the OPLS-AA Force Field. *J. Chem. Theory Comput.* **2015**, *11* (7), 3499–3509. https://doi.org/10.1021/acs.jctc.5b00356.

(56) Vanquelef, E.; Simon, S.; Marquant, G.; Garcia, E.; Klimerak, G.; Delepine, J. C.; Cieplak, P.; Dupradeau, F.-Y. R.E.D. Server: A Web Service for Deriving RESP and ESP Charges and Building Force Field Libraries for New Molecules and Molecular Fragments. *Nucleic Acids Res.* **2011**, *39*, W511–W517. https://doi.org/10.1093/nar/gkr288.

(57) Girifalco, L. A. Molecular Properties of C_{60} in the Gas and Solid Phases. *J. Phys. Chem.* **1992**, *96* (2), 858–861. https://doi.org/10.1021/j100181a061.

(58) Huang, Z. R.; Hua, S. C.; Yang, Y. L.; Fang, J. Y. Development and Evaluation of Lipid Nanoparticles for Camptothecin Delivery: A Comparison of Solid Lipid Nanoparticles, Nanostructured Lipid Carriers, and Lipid Emulsion. *Acta Pharmacol. Sin.* **2008**, *29* (9), 1094–1102. https://doi.org/10.1111/j.1745-7254.2008.00829.x.

(59) Senge, M. O.; Brandt, J. C. Temoporfin (Foscan®, 5,10,15,20-Tetra(m-Hydroxyphenyl)Chlorin) - A Second-Generation Photosensitizer. *Photochemistry and Photobiology*. November 2011, pp 1240–1296. https://doi.org/10.1111/j.1751-1097.2011.00986.x.

(60) Golomidov, I.; Bolshakova, O.; Komissarov, A.; Sharoyko, V.; Slepneva, E.; Slobodina, A.; Latypova, E.; Zherebyateva, O.; Tennikova, T.; Sarantseva, S. The Neuroprotective Effect of Fullerenols on a Model of Parkinson's Disease in Drosophila Melanogaster. *Biochem. Biophys. Res. Commun.* **2020**, *523* (2), 446–451.

https://doi.org/10.1016/j.bbrc.2019.12.075.

(61) Grebowski, J.; Konopko, A.; Krokosz, A.; DiLabio, G. A.; Litwinienko, G. Antioxidant Activity of Highly Hydroxylated Fullerene C_{60} and Its Interactions with the Analogue of α-Tocopherol. *Free Radic. Biol. Med.* **2020**, *160*, 734–744. https://doi.org/10.1016/j.freeradbiomed.2020.08.017.

(62) Srdjenovic, B.; Milic-Torres, V.; Grujic, N.; Stankov, K.; Djordjevic, A.; Vasovic, V. Antioxidant Properties of Fullerenol $C_{60}(OH)_{24}$ in Rat Kidneys, Testes, and Lungs Treated with Doxorubicin. *Toxicol. Mech. Methods* **2010**, *20* (6), 298–305. https://doi.org/10.3109/15376516.2010.485622.

(63) Kovel, E. S.; Sachkova, A. S.; Vnukova, N. G.; Churilov, G. N.; Knyazeva, E. M.; Kudryasheva, N. S. Antioxidant Activity and Toxicity of Fullerenols via Bioluminescence Signaling: Role of Oxygen Substituents. *Int. J. Mol. Sci.* **2019**, *20* (9), 2324. https://doi.org/10.3390/ijms20092324.

(64) He, X. M.; Carter, D. C. Atomic Structure and Chemistry of Human Serum Albumin. *Nature* **1992**, *358* (6383), 209–215. https://doi.org/10.1038/358209a0.

(65) Tang, J.; Luan, F.; Chen, X. Binding Analysis of Glycyrrhetinic Acid to Human Serum Albumin: Fluorescence Spectroscopy, FTIR, and Molecular Modeling. *Bioorg. Med. Chem.* **2006**, *14* (9), 3210–3217. https://doi.org/10.1016/j.bmc.2005.12.034.

(66) Ungurenasu, C.; Pinteala; Dascalu. Binding Fullerenol C60(OH)24 to DsDNA. *Int. J. Nanomedicine* **2009**, *4*, 193. https://doi.org/10.2147/ijn.s6630.

(67) Mrđanović, J.; Šolajić, S.; Bogdanović, V.; Stankov, K.; Bogdanović, G.; Djordjevic, A. Effects of Fullerenol $C_{60}(OH)_{24}$ on the Frequency of Micronuclei and Chromosome Aberrations in CHO-K1 Cells. *Mutat. Res. Toxicol. Environ. Mutagen.* **2009**, *680* (1–2), 25–30. https://doi.org/10.1016/J.MRGENTOX.2009.08.008.

(68) Serebryakov, E. B.; Zakusilo, D. N.; Semenov, K. N.; Charykov, N. A.; Akentiev, A.

V.; Noskov, B. A.; Petrov, A. V.; Podolsky, N. E.; Mazur, A. S.; Dul'neva, L. V. et al. Physico-Chemical Properties of C_{70}-L-Threonine Bisadduct ($C_{70}(C_4H_9NO_2)_2$) Aqueous Solutions. *J. Mol. Liq.* **2019**, *279*, 687–699. https://doi.org/10.1016/j.molliq.2019.02.013.

1 Table 1. Provenance and mass fraction purity of the reagents.

№	Sample	Manufacturer	Main substance content
1	$C_{60}(OH)_{24}$	Ltd ZAO “ILIP”, Russia	≥0.998
2	HSA	Biolot, Russia	≥0.950
3	PBS	Biolot, Russia	
4	Radachlorin	Rada-Pharma, Russia	
5	Dimethyl sulphoxide	Sigma-Aldrich, USA	≥0.997
6	Sodium azide	Sigma-Aldrich, USA	≥0.995
7	ADP	Sigma-Aldrich, USA	≥0.950
8	Sodium citrate	Sigma-Aldrich, USA	≥0.999
9	Propidium iodide	Sigma-Aldrich, USA	≥0.940
10	Hydrogen peroxide	Biolot, Russia	≥0.333
11	Digitonin	Sigma-Aldrich, USA	≥0.920
12	Ibuprofen	Sigma-Aldrich, USA	≥0.980
13	Warfarin	Sigma-Aldrich, USA	≥0.970
14	DNA from salmon sperm with an average mass of 350 kDa (by gel electrophoresis)	Technomedservice, Russia	≥0.980

2

Table 2. Size distribution of $C_{60}(OH)_{24}$ associates in aqueous solutions at 293.15 K. δ_i is average diameters of *i*-th order molecules in the solution; $N_{0\to1}$ is average numbers of $C_{60}(OH)_{24}$ monomeric molecules in clusters of the first order. Calculation of the content of the monomeric molecules in first-order associates was performed using the equation $N_{0\to i} = \left(\frac{\delta_i}{\delta_0}\right)^3 \cdot \left(K_{pack}\right)^i$, where δ_0 is the diameter of $C_{60}(OH)_{24}$ molecule, K_{pack} is the packing coefficient corresponding to the packing of "small spheres" into the "big sphere" (in our case, the value of $K_{pack} = 0.52$ was chosen) [68]; ζ is the zeta potential of the associates [40,42].

C / μM	δ_i / nm	$N_{0\to1}$	ζ / mV
0	2 [41]	—	—
10	10	$\approx 6\cdot10^1$	−30
50	20	$\approx 5\cdot10^2$	−30
75	40	$\approx 4\cdot10^3$	−30
100	40	$\approx 4\cdot10^3$	−30

Table 3. Indicators of coagulation haemostasis following the addition of $C_{60}(OH)_{24}$ to human plasma.

			C / μM			
	Standard	Control	10	50	75	100
Test type	Coagulation time / s					
TT / s	15–19	17.1 ± 1.6	16.2 ± 1.3	40 ± 1.2*	42.6 ± 1.8*	>120.0
aPTT / s	28–40	36.5 ± 1.9	46.3 ± 0.9*	65.2 ± 0.8*	66.8 ± 0.7*	68.4 ± 1.6*
PT / s	13–18	13.6 ± 1.8	15.0 ± 1.0	16.5 ± 1.3*	21.2 ± 1.5*	20.1 ± 1.2*

*$p < 0.05$ relative to control.

Table 4. The values of the photobleaching constant of Radachlorin in the presence of NaN_3 and $C_{60}(OH)_{24}$.

Agent	C / μM	K_{deg} / s^{-1}
—	—	0.0308 ± 0.0004
$C_{60}(OH)_{24}$	10	0.0295 ± 0.0006
$C_{60}(OH)_{24}$	50	0.0235 ± 0.0005
$C_{60}(OH)_{24}$	75	0.0219 ± 0.0005
$C_{60}(OH)_{24}$	100	0.0191 ± 0.0002
NaN_3	500	0.0023 ± 0.0001

Table 5. The effect of $C_{60}(OH)_{24}$ on platelet aggregation in the presence of ADP.

Amplitude / %				
Concentration of $C_{60}(OH)_{24}$ / μM				
Control	10	50	75	100
83.4 ± 7.32	77.50 ± 4.16	76.57 ± 5.28	56.87 ± 5.28*	59.5 ± 5.91*

*$p < 0.05$ relative to control.

Table 6. The logarithms of the binding constants ($\lg K_b$) and the stoichiometry of the binding reaction (n) of $C_{60}(OH)_{24}$ to HSA.

Site marker	$C = 3 \cdot 10^{-7}$–$1.5 \cdot 10^{-6}$ M		$C = 6 \cdot 10^{-6}$–$2.4 \cdot 10^{-5}$ M	
	$\lg K_b$ / $\lg M^{-1}$	n	$\lg K_b$ / $\lg M^{-1}$	n
No markers	5.4 ± 0.2	1.02 ± 0.03	2.9 ± 0.2	0.56 ± 0.03
Warfarin	5.2 ± 0.2	0.97 ± 0.03	3.3 ± 0.2	0.61 ± 0.04
Ibuprofen	5.1 ± 0.2	0.95 ± 0.04	1.0 ± 0.1	0.15 ± 0.02
Digitonin	4.5 ± 0.3	0.88 ± 0.05	3.0 ± 0.3	0.52 ± 0.04

Table 7. Correlation parameters of Eq. 3 applied for determining the dissociation constant of $C_{60}(OH)_{24}$–HSA complex.

Parameter	$C = 0–1.6 \cdot 10^{-6}$ M	$C = 3.13 \cdot 10^{-6}–10^{-4}$ M
B_{max} / °C	3866	–962.3
NS / °C·M^{-1}	−83253674	408375
B / °C	86.13	88.97

1 Table 8. The thermodynamic parameters of the $C_{60}(OH)_{24}$ binding to DNA and the number of

2 binding sites in the temperature range 303.15–318.15 K.

T / K	n	$K_b \cdot 10^3$ / M^{-1}	ΔG / kJ·mol^{-1}	ΔH / kJ·mol^{-1}	ΔS / J·K^{-1}·mol^{-1}
303.15	0.76 ± 0.04	1.8 ± 0.1	−19.0 ± 3.2		
308.15	0.86 ± 0.04	4.8 ± 0.3	−21.3 ± 3.5	115 ± 15	443 ± 46
313.15	0.89 ± 0.03	6.7 ± 0.3	−23.5 ± 3.9		
318.15	0.98 ± 0.07	17.9 ± 1.4	−25.7 ± 4.3		

3

Table 9. The effect of $C_{60}(OH)_{24}$ on % tail DNA, tail length, and tail moment.

		Amplitude / %				
Characteristic studied	Negative control	Concentration of H_2O_2 / µM	Concentration of $C_{60}(OH)_{24}$ / µM			
		100.0	10.0	50.0	75.0	100.0
% tail DNA	0.84 ± 0.38	82.14 ± 2.03***	5.70 ± 1.85**	13.18 ± 3.26**	17.84 ± 2.60**	22.47 ± 3.50**
Tail length	28.59 ± 4.27	646.63 ± 67.67**	15.08 ± 3.81	25.08 ± 4.51	31.10 ± 6.93	25.25 ± 5.95
Tail moment	0.24 ± 0.08	531.14 ± 19.89***	0.85 ± 0.28*	3.30 ± 0.43**	5.54 ± 0.40**	5.67 ± 0.21**

*$p < 0.05$ relative to negative control.

**$p < 0.01$ relative to negative control.

***$p < 0.001$ relative to negative control.

1 Table 10. The average number of hydrogen bonds in the complex of HSA with $C_{60}(OH)_{24}$.

Isomer	DS1	DS2	DS3	Surface 1	Surface 2
Uniform	4.0 ± 1.3	3.0 ± 1.6	4.0 ± 1.6	8.5 ± 2.3	2.7 ± 1.3
Saturn-like	4.9 ± 1.3	7.4 ± 1.5	3.1 ± 2.0	7.2 ± 1.9	3.6 ± 1.8

2

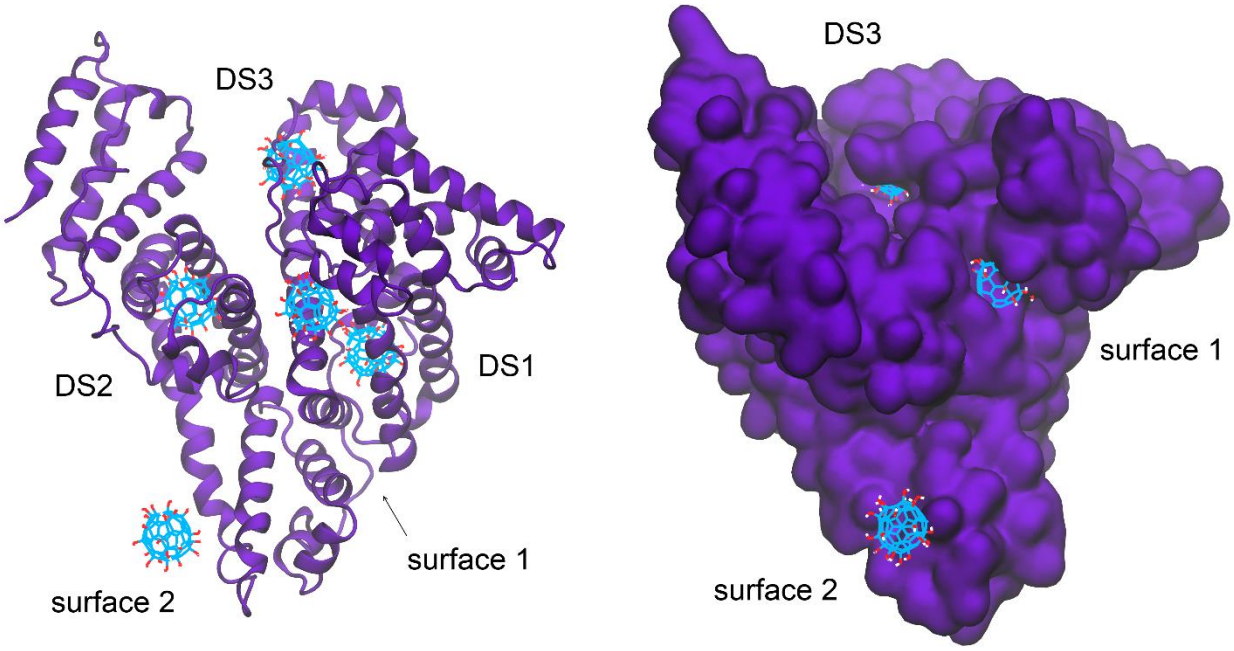

1

2 Fig. 1. The positions of the $C_{60}(OH)_{24}$ molecule (the uniform isomer) in binding sites of HSA

3 in the initial configurations for MD simulations.

4

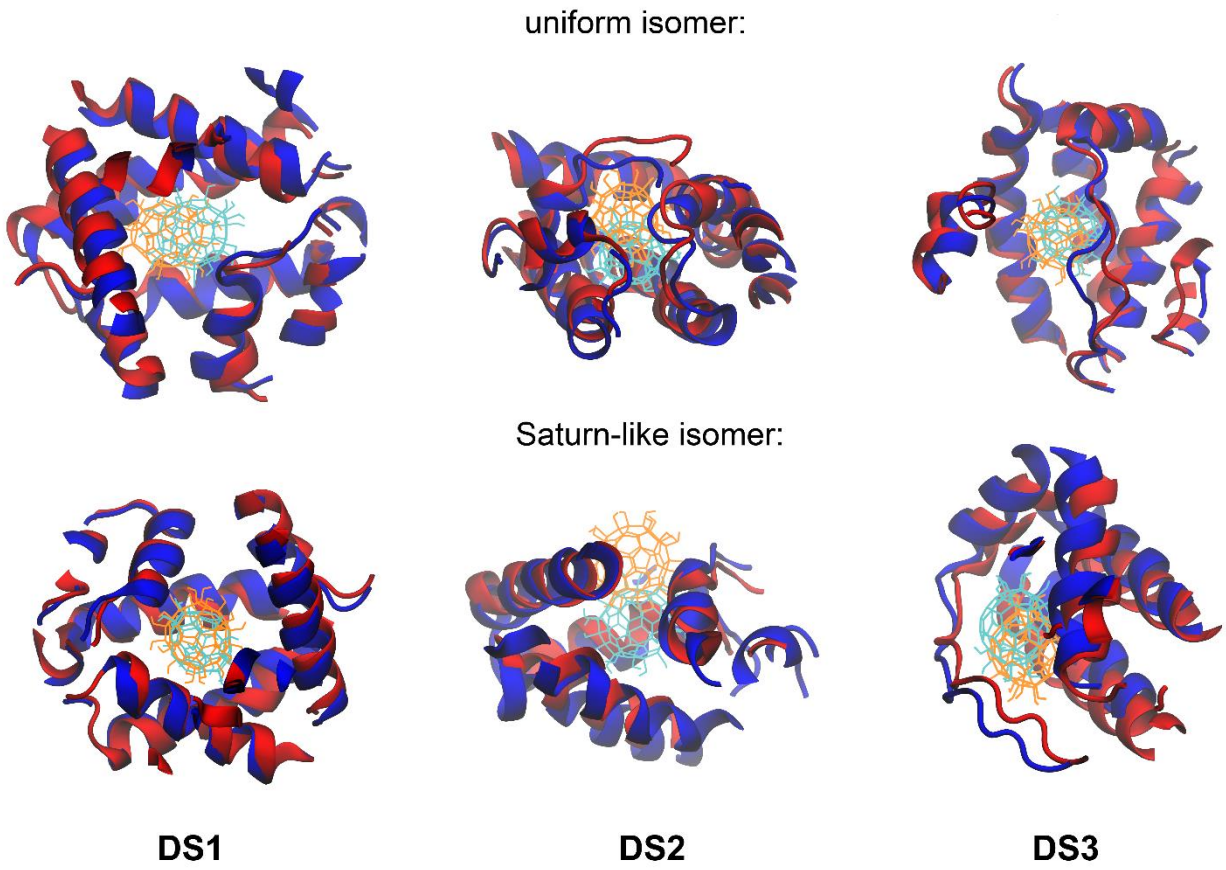

Fig. 2. The displacement of the fullerenol $C_{60}(OH)_{24}$ after 20 ns of MD simulation. The initial configurations (at 0 ns) are coloured in red and orange, the final ones (at 20 ns) are coloured in blue. The two configurations are fitted to minimise the root-mean square displacement of the docking site, not the whole protein, between 0 ns and 20 ns. Only 1–1.5 nm vicinity of the fullerenol is shown for clarity. The view direction is chosen to maximally show all the magnitude of the fullerenol displacement.

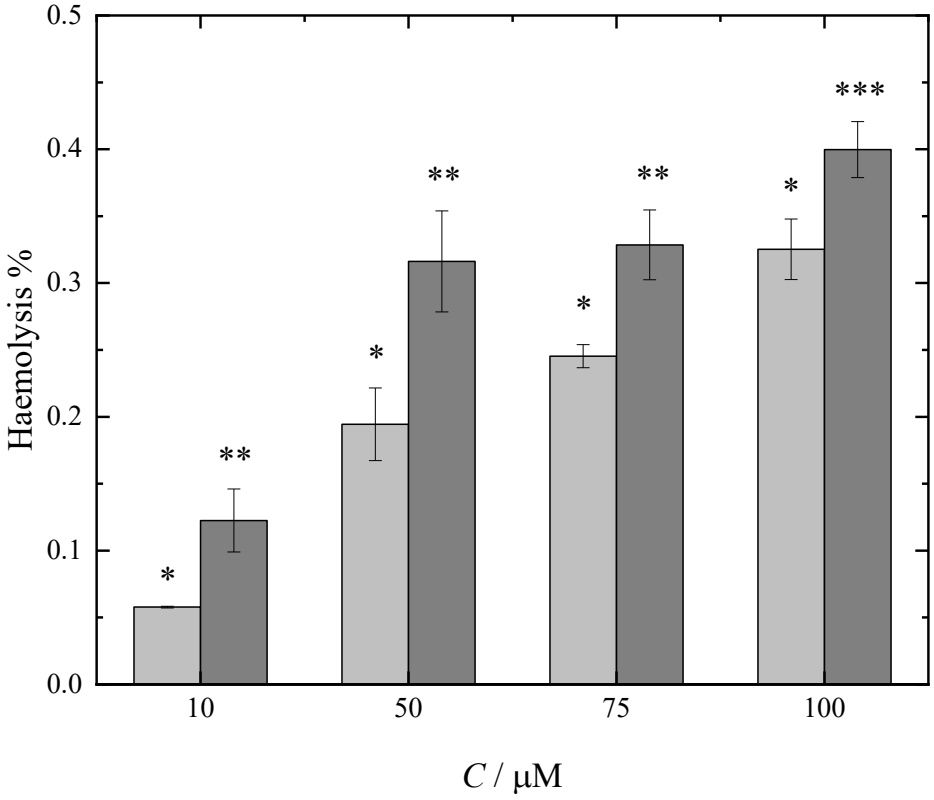

Fig. 3. The effect of $C_{60}(OH)_{24}$ on the degree of erythrocyte haemolysis after 1 h (light grey) and 3 h (dark grey) of incubation. *C* is the molar concentration of $C_{60}(OH)_{24}$.

*$p < 0.05$ relative to control (1 h).

**$p < 0.05$ relative to negative control (3 h).

***p < 0.01 relative to control (3 h).

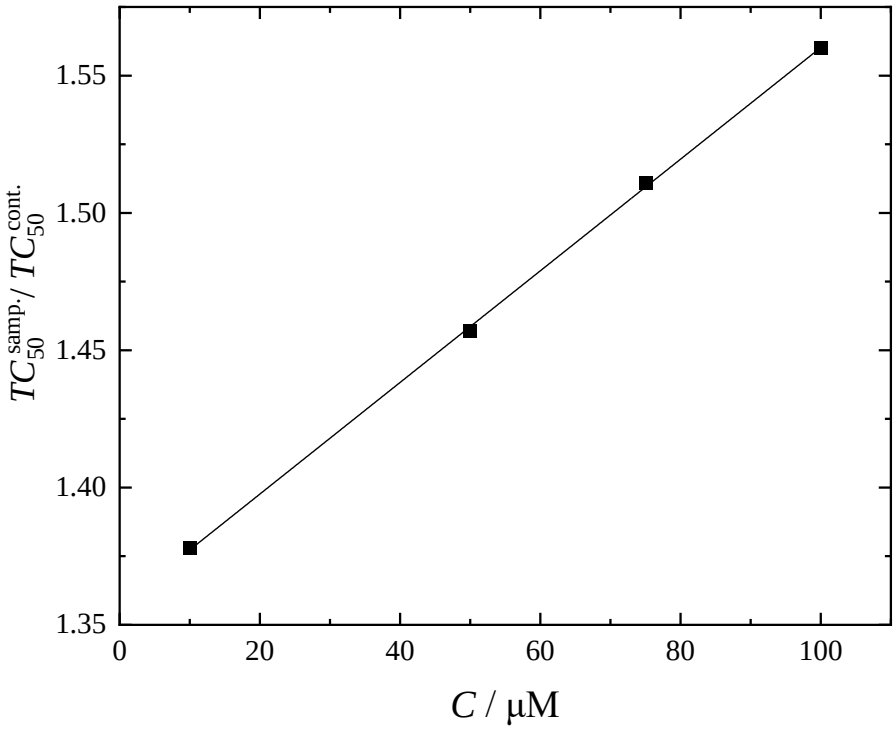

1

2 Fig. 4. The concentration dependence of the degree of photo-induced haemolysis in the
3 presence of $C_{60}(OH)_{24}$. C is molar concentration of fullerenol, $TC_{50}^{samp.}$ is the time of photo-
4 induced haemolysis of 50 % of erythrocytes in the presence of $C_{60}(OH)_{24}$, $T_{50}^{cont.}$ is the time of
5 photo-induced haemolysis of 50 % of erythrocytes in the presence of physiological saline
6 (control).

7

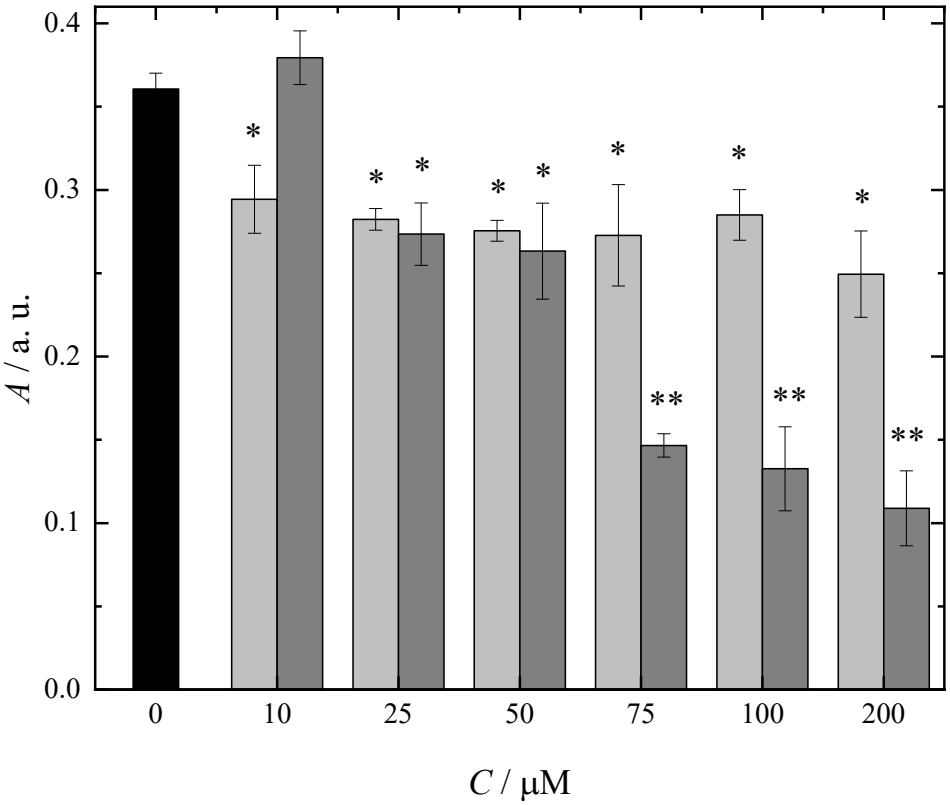

Fig. 5. Effect of $C_{60}(OH)_{24}$ (light grey) and sodium azide (dark grey) on NO-radical uptake.

*$p < 0.05$ relative to control.

**$p < 0.01$ relative to control.

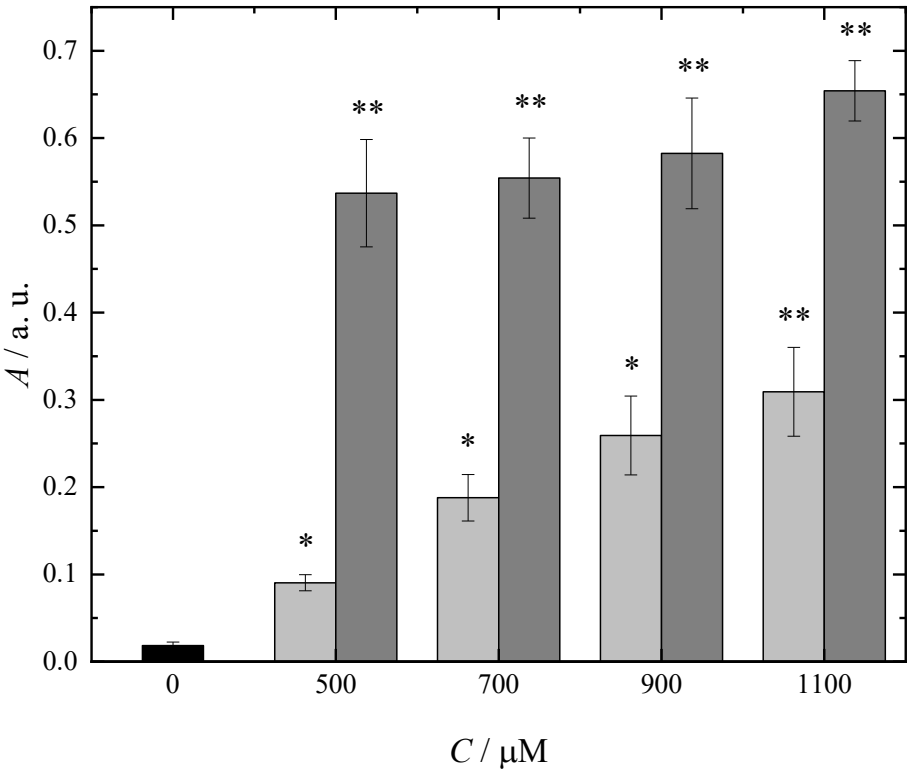

Fig. 6. The reducing capacity of $C_{60}(OH)_{24}$ (light grey) and ascorbic acid (dark grey).

*$p < 0.05$ relative to control.

**$p < 0.01$ relative to control.

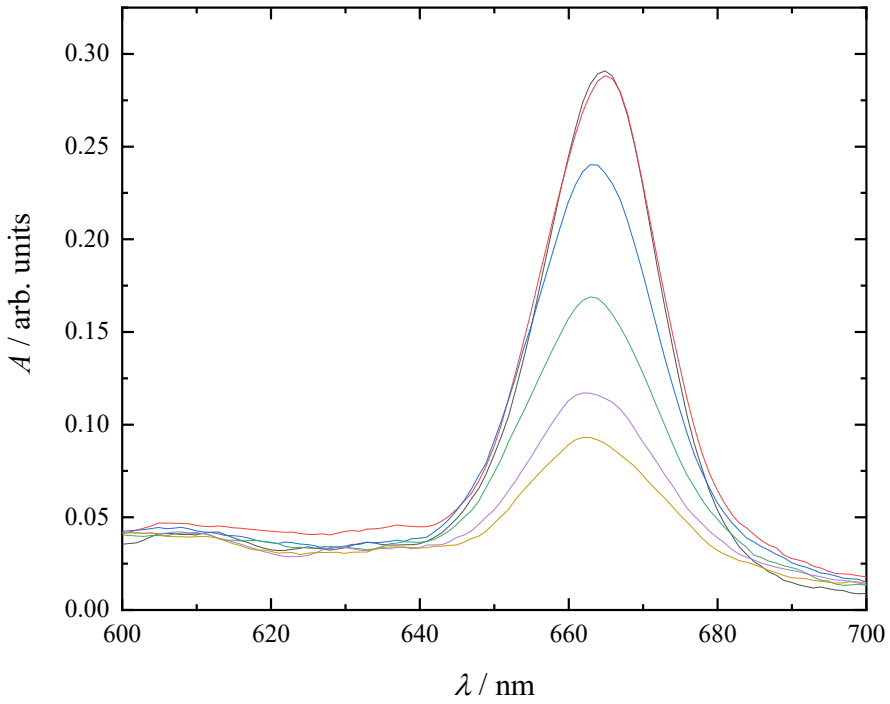

1

2 Fig. 7. Absorption spectra of Radachlorin + $C_{60}(OH)_{24}$ (C = 2.5 mg·l^{-1}) without irradiation (—

3) and under irradiation (— 10 s, — 20 s, — 30 s, — 40 s, — 50 s).

4

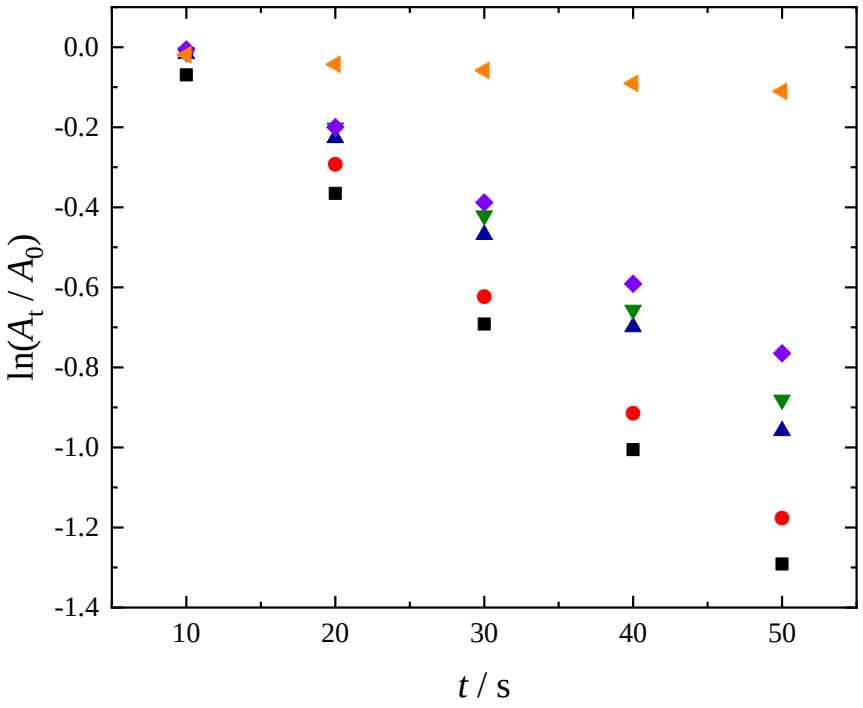

Fig. 8. Kinetic dependence of photobleaching of Radachlorin (■) in the presence of $C_{60}(OH)_{24}$ (● 10 μM, ▲ 50 μM, ▼ 75 μM, ◆ 100 μM) and NaN_3 (◀ 500 μM). A_t and A_0 are the optical densities of Radachlorin solutions at 659 nm before and after irradiation.

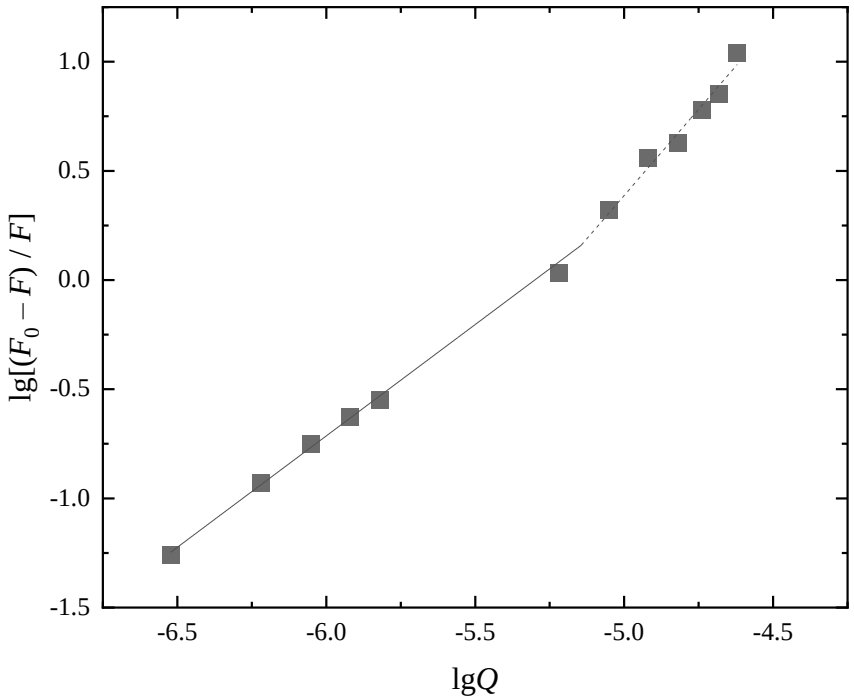

Fig. 9. Dependence of the binding process of $C_{60}(OH)_{24}$ to HSA at 298.15 K in the absence of binding site markers in Hill coordinates. F_0 is HSA fluorescence intensity in the absence of $C_{60}(OH)_{24}$, F is HSA fluorescence intensity in the presence of $C_{60}(OH)_{24}$, Q is the molar concentration of $C_{60}(OH)_{24}$.

(*a*)

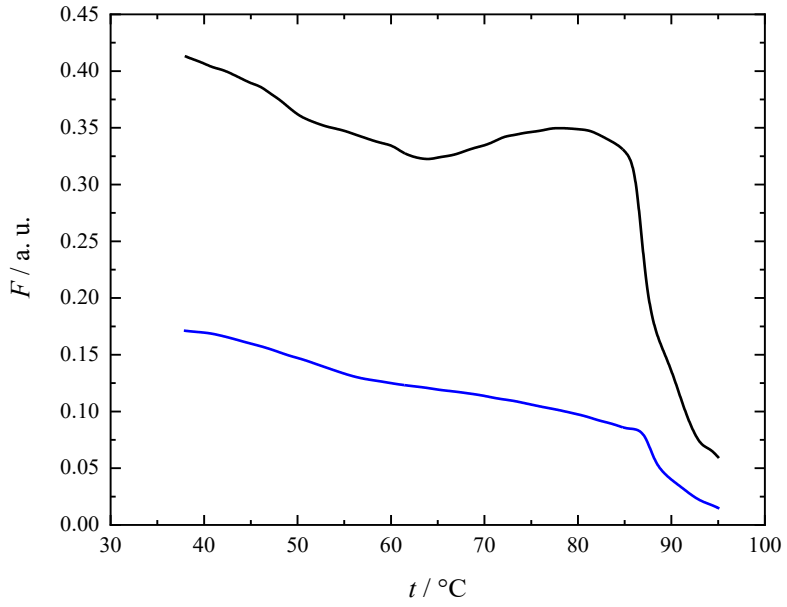

(*b*)

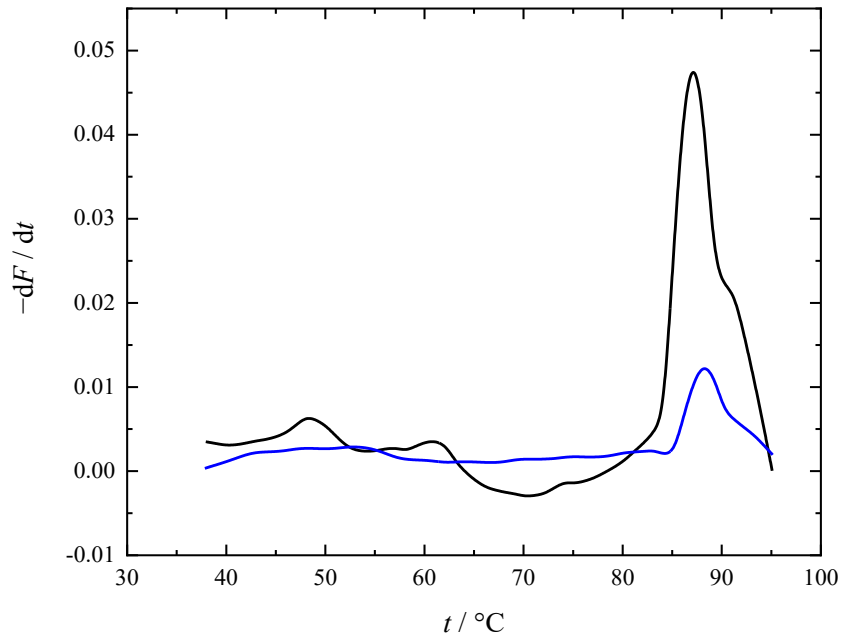

Fig. 10. Temperature dependence of fluorescence (*a*) and its first derivative (*b*) for $C_{60}(OH)_{24}$–HSA complex (blue line, $C = 10^{-4}$ M) in comparison to pure HSA (black line).

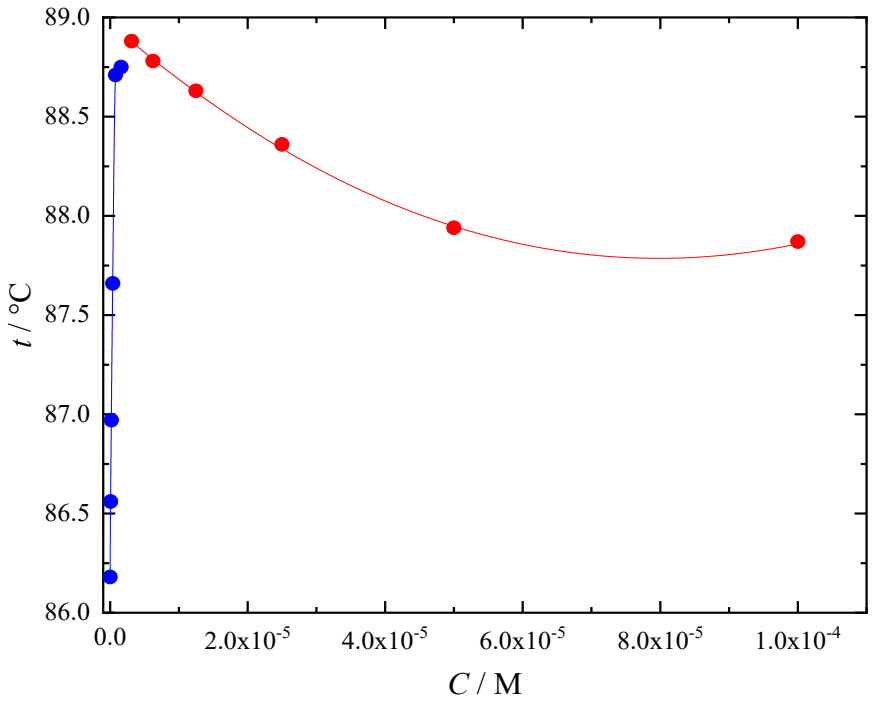

1

2 Fig. 11. Dependence of fullerenol concentration on $C_{60}(OH)_{24}$–HSA complex melting point.

3

(*a*)

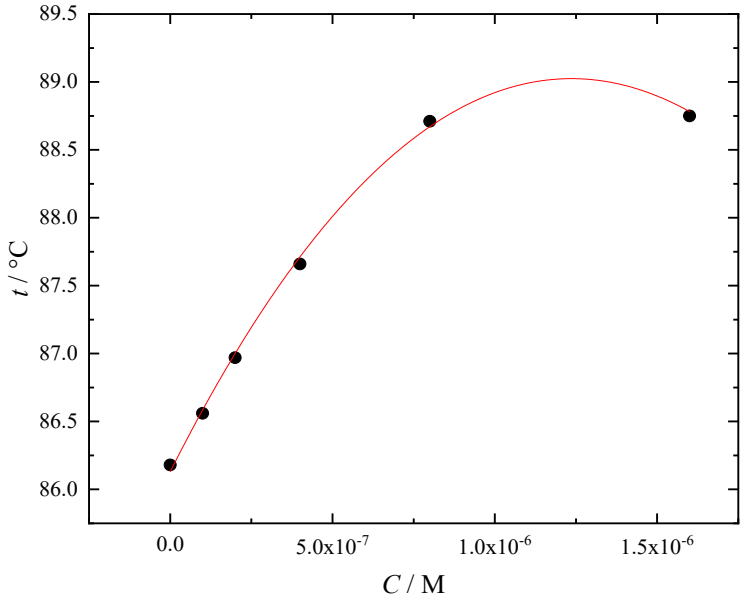
89.5
89.0
88.5
88.0
87.5
87.0
86.5
86.0
t / °C
0.0
5.0x10-7
1.0x10-6
1.5x10-6
C / M

(*b*)

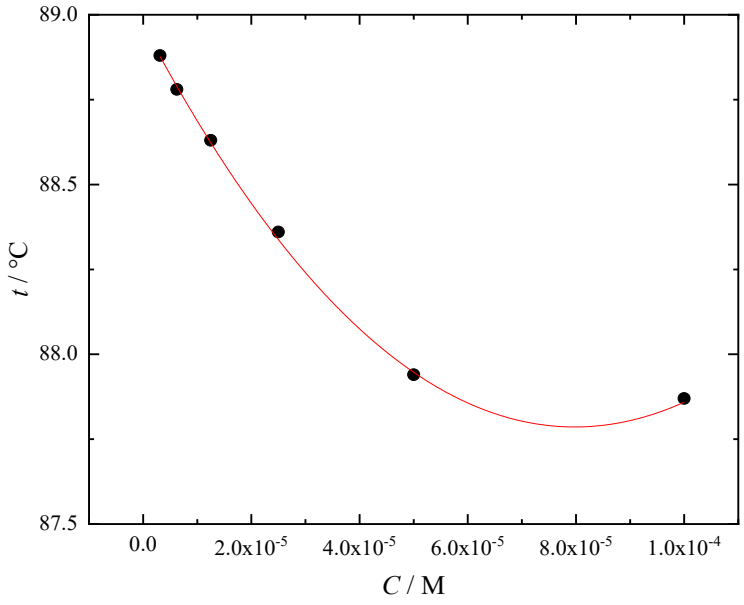
89.0
88.5
88.0
87.5
t / °C
0.0
2.0x10-5
4.0x10-5
6.0x10-5
8.0x10-5
1.0x10-4
C / M

Fig. 12. The concentration dependence of the melting point of $C_{60}(OH)_{24}$–HSA complex in the concentration ranges C = 0–$1.6 \cdot 10^{-6}$ M (binding to digitonin, *a*) and C = $3.13 \cdot 10^{-6}$–10^{-4} M (binding to ibuprofen, *b*). Dots are experimental values; lines represent the approximation by Eq. 3.

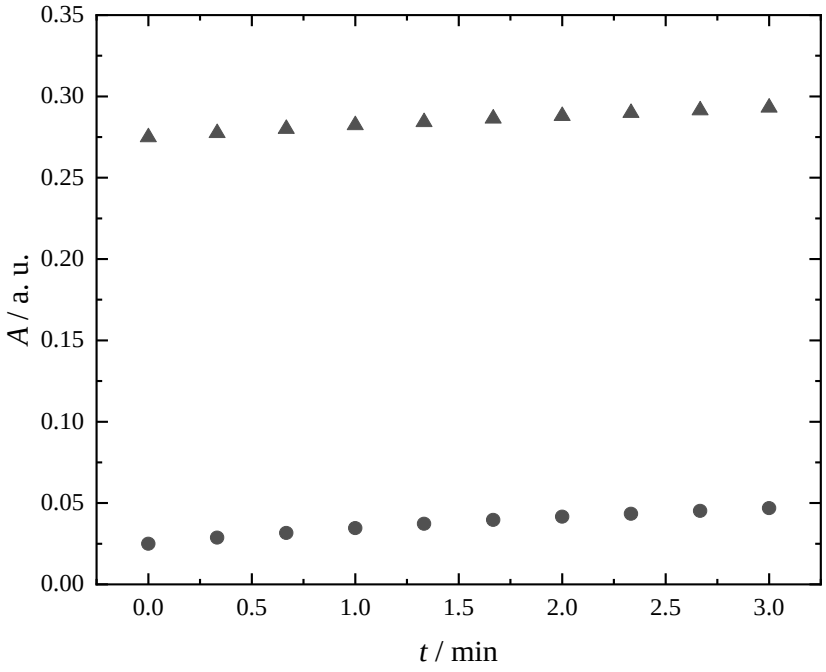

1

2 Fig. 13. Kinetic dependences of the hydrolysis reaction of NPA with HSA in the absence (●)

3 and in the presence of 24 μM $C_{60}(OH)_{24}$ (▲).

4

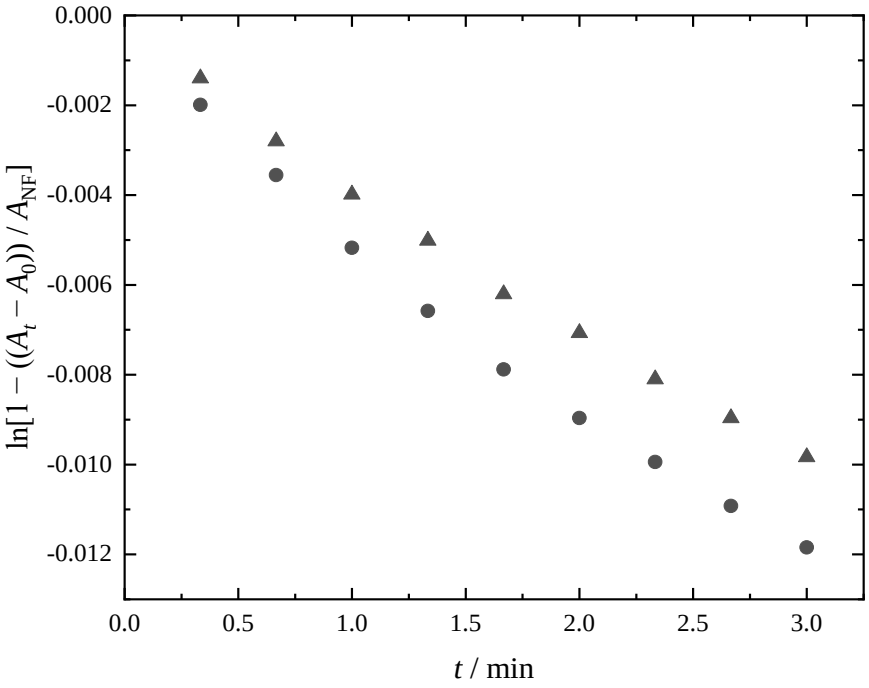

1

2 Fig. 14. Dependencies $\ln\left(1-\frac{A_t - A_0}{A_{NF}}\right)$ on time for reaction of hydrolysis of NPA with HSA

3 in the absence (●) and in the presence of 24 μM $C_{60}(OH)_{24}$ (▲).

4

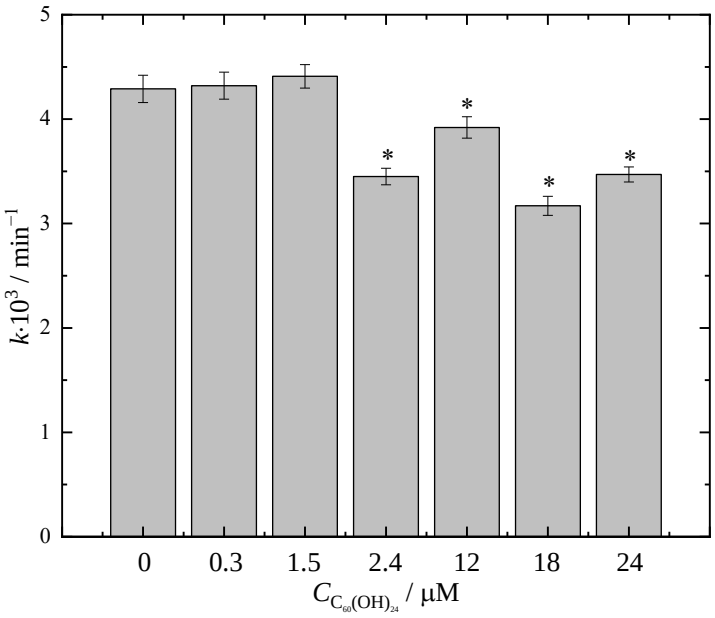

Fig. 15. Values of the rate constants of the hydrolysis reaction of NPA with HSA in the concentration range of $C_{60}(OH)_{24}$ 0–24 μM.

*$p < 0.05$ relative to control (in the absence of $C_{60}(OH)_{24}$).

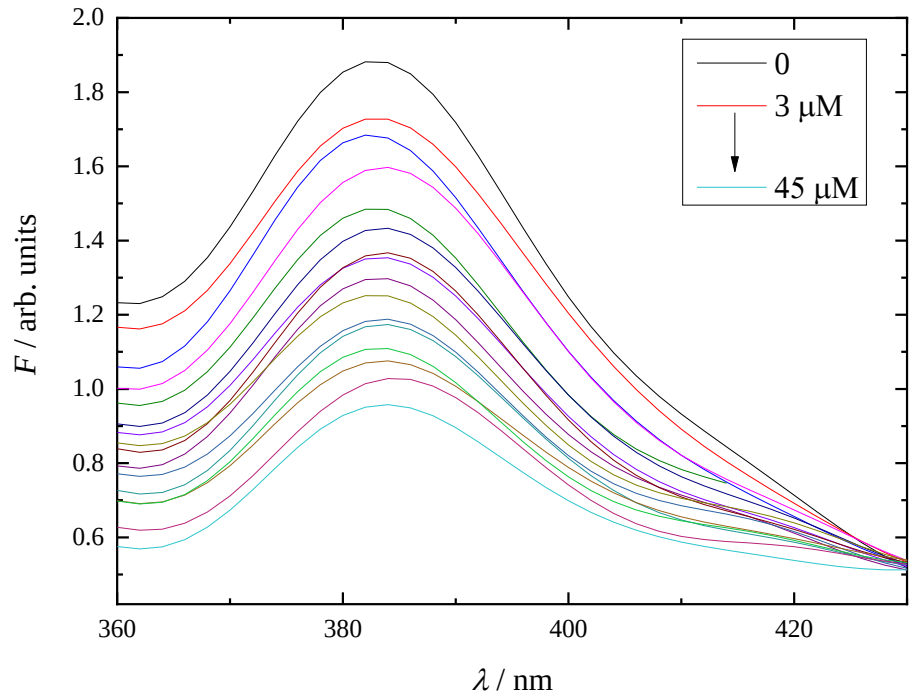

Fig. 16. DNA fluorescence spectra in the absence and presence of $C_{60}(OH)_{24}$ (C = 3–45 μM) at 303.15 K.

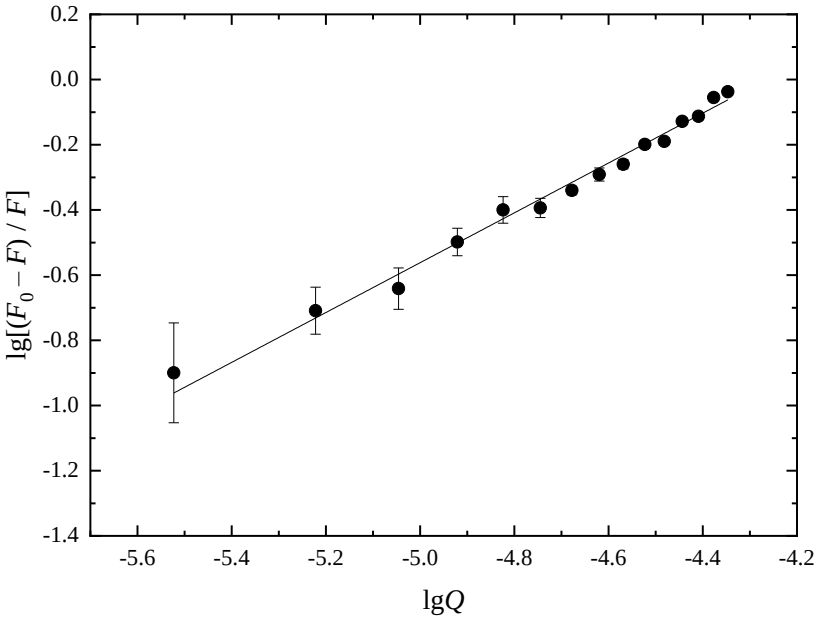

1

2 Fig. 17. Dependence of the $C_{60}(OH)_{24}$ binding process to DNA at 303.15 K in Hill coordinates.

3

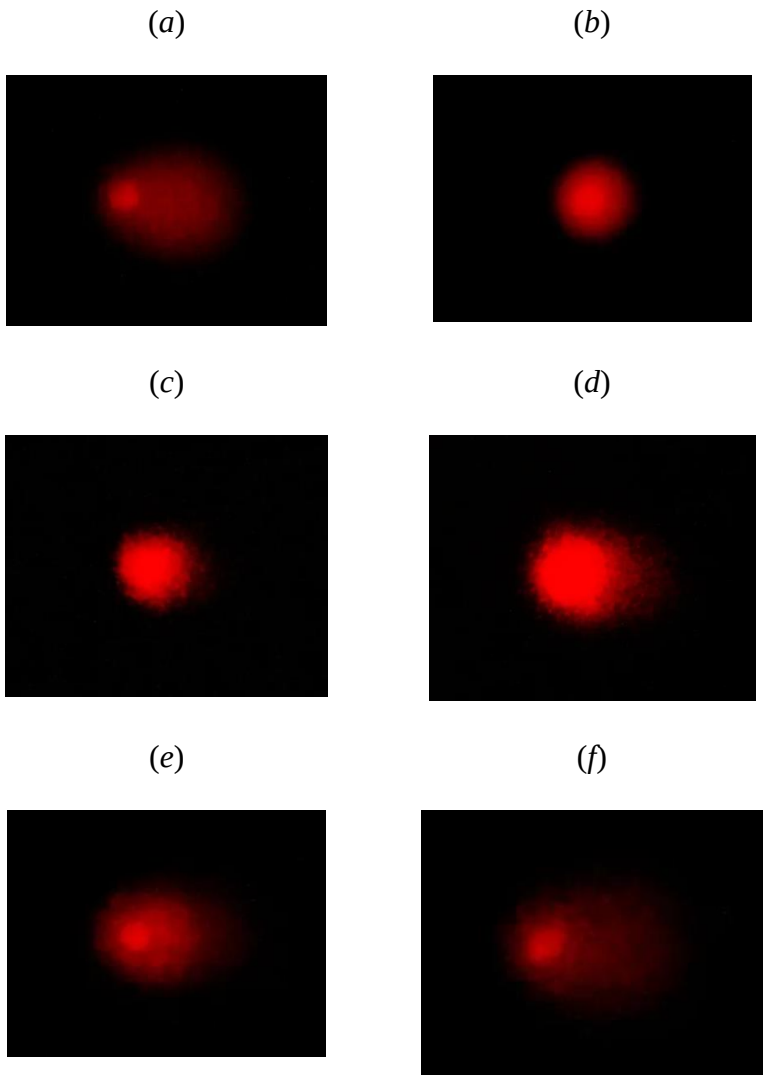

Fig. 18. Photographs of DNA comets after electrophoresis of cells in a microgel. (*a*) — positive control (H_2O_2), (*b*) — negative control (PBS), (*c*–*f*) — $C_{60}(OH)_{24}$ (*C* = 10, 50, 75 and 100 μM).

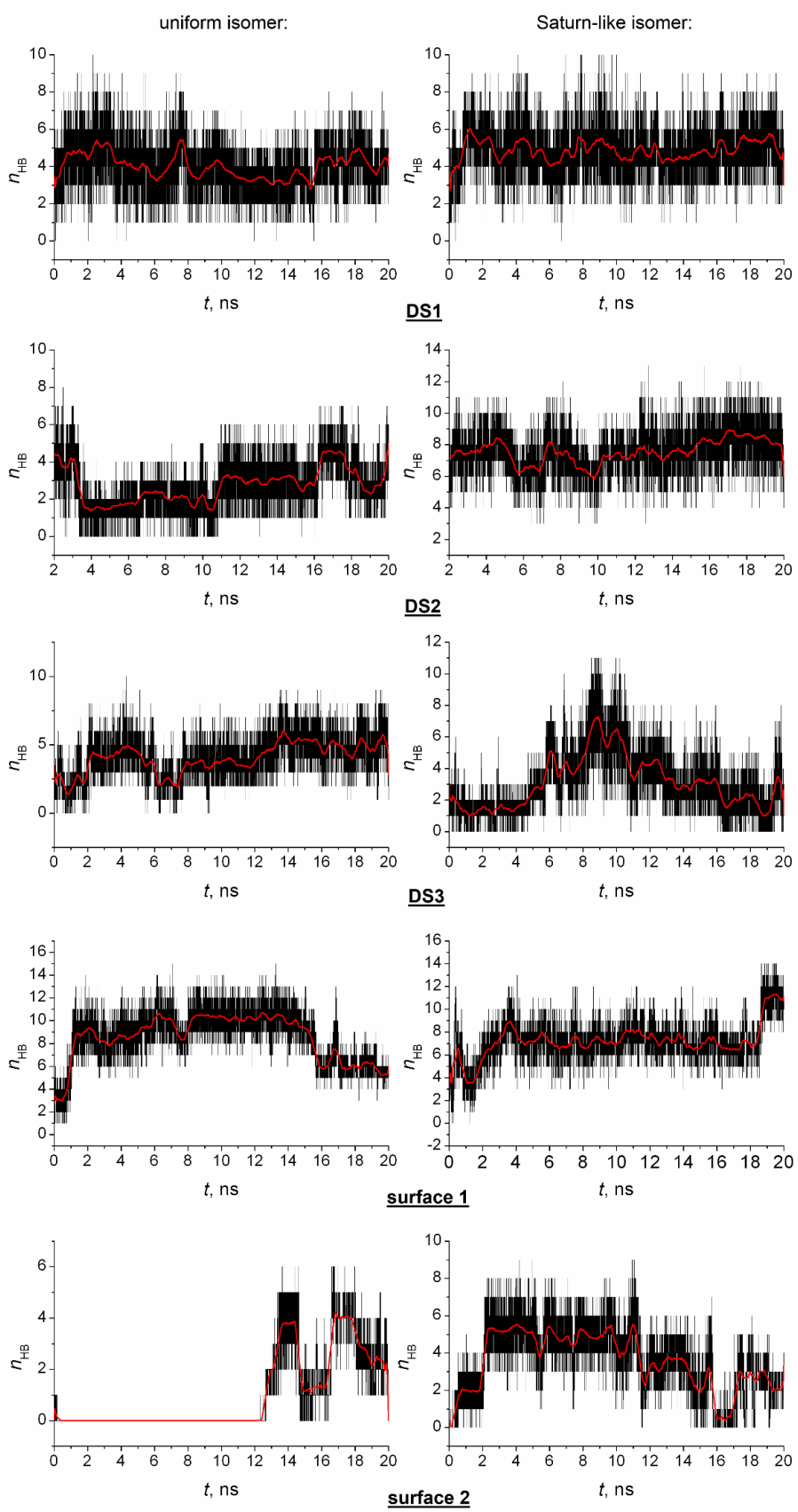

Fig. 19. The number of hydrogen bonds between HSA and fullerenol $C_{60}(OH)_{24}$ during simulation. Red curve is the result of smoothing.